AM. Interestingly, the hemodynamic effects of inhaled AM lasted for >45 minutes. A previous study demonstrated that intravenous injection of AM produces a long-lasting vasodilator response because of its long half-life (≈15 minutes).[32] The half-life of plasma AM after inhalation was longer (20 minutes). Thus, inhalation of AM may cause relatively long-lasting pulmonary vasodilator activity in patients with idiopathic pulmonary arterial hypertension. In the present study, plasma cAMP level increased after AM inhalation, suggesting that the hemodynamic effects of AM may be mediated by activation of cAMP.

Earlier studies have shown that peak $\dot{V}o_2$ during exercise is markedly lower in patients with idiopathic pulmonary arterial hypertension than in healthy subjects.[33,34] Peak $\dot{V}o_2$ is determined primarily by the maximal cardiac output during exercise and the potential for O_2 extraction by the exercising muscle.[35] Thus, the decreased peak $\dot{V}o_2$ may reflect insufficient oxygen delivery to the body during exercise, at least in part because of an inadequate increase in cardiac output under conditions of severe pulmonary hypertension. In the present study, inhalation of AM significantly increased peak $\dot{V}o_2$ in patients with pulmonary hypertension. AM also increased the $\Delta\dot{V}o_2/\Delta W$ ratio, which indicates oxygen transport per unit workload to the exercising legs. These results suggest that inhalation of AM improves exercise capacity in patients with idiopathic pulmonary arterial hypertension. It is possible that an increase in cardiac output during exercise may contribute to increases in peak $\dot{V}o_2$ and the $\Delta\dot{V}o_2/\Delta W$ ratio.

The major limitation of this pilot trial relates to the lack of a randomized, placebo-controlled group in acute hemodynamic studies, which was as result not only of invasive assessment of hemodynamics but also of the limited number of patients available. Nevertheless, cardiopulmonary exercise testing was performed in a double-blind, randomized, crossover design. Thus, it is unlikely that the hemodynamic effects of inhaled AM are attributable to the placebo effect.

Inhalation therapy may be more simple, noninvasive, and comfortable than continuous intravenous infusion therapy. An experimental study demonstrated that repeated inhalation of AM (for 30 minutes, 4 times a day) inhibited monocrotaline-induced pulmonary hypertension and markedly improved survival in rats.[36] Recently, pulmonary delivery of a dry-powder insulin has been shown to improve glycemic control without adverse pulmonary effects.[37] Although further studies are necessary to maximize the efficiency and reproducibility of pulmonary AM delivery, combining AM inhalation therapy with other modalities that have a different mode of action may have beneficial effects in patients with idiopathic pulmonary arterial hypertension.

Conclusions

These preliminary results suggest that inhalation of AM may have beneficial effects on pulmonary hemodynamics and exercise capacity in patients with idiopathic pulmonary arterial hypertension.

Acknowledgments

This work was supported by grants from NEDO, the Mochida Memorial Foundation for Medical and Pharmaceutical Research, the Japan Cardiovascular Research Foundation, Health and Labor Sciences Research grant genome 005, and the Promotion of Fundamental Studies in Health Science of the Organization for Pharmaceutical Safety and Research of Japan. We thank Masahiko Shibakawa for preparing AM.

References

1. Rich S, Dantzker DR, Ayres SM, et al. Primary pulmonary hypertension: a national prospective study. *Ann Intern Med.* 1987;107:216–223.
2. Rich S. Primary pulmonary hypertension. *Prog Cardiovasc Dis.* 1988;31:205–238.
3. Rubin LJ, Peter RH. Oral hydralazine therapy for primary pulmonary hypertension. *N Engl J Med.* 1980;302:69–73.
4. Rich S, Kaufmann E, Levy PS. The effect of high doses of calcium-channel blockers on survival in primary pulmonary hypertension. *N Engl J Med.* 1992;327:76–81.
5. Barst RJ, Rubin LJ, Long WA, et al. A comparison of continuous intravenous epoprostenol (prostacyclin) with conventional therapy for primary pulmonary hypertension. *N Engl J Med.* 1996;334:296–301.
6. McLaughlin VV, Genthner DE, Panella MM, et al. Reduction in pulmonary vascular resistance with long-term epoprostenol (prostacyclin) therapy in primary pulmonary hypertension. *N Engl J Med.* 1998;338:273–277.
7. Nagaya N, Uematsu M, Okano Y, et al. Effect of orally active prostacyclin analogue on survival of outpatients with primary pulmonary hypertension. *J Am Coll Cardiol.* 1999;34:1188–1192.
8. Reitz BA, Wallwork JL, Hunt SA, et al. Heart-lung transplantation: successful therapy for patients with pulmonary vascular disease. *N Engl J Med.* 1982;306:557–564.
9. Pasque MK, Trulock EP, Kaiser LD, et al. Single lung transplantation for pulmonary hypertension: three month hemodynamic follow-up. *Circulation.* 1991;84:2275–2279.
10. Kitamura K, Kangawa K, Kawamoto M, et al. Adrenomedullin: a novel hypotensive peptide isolated from human pheochromocytoma. *Biochem Biophys Res Commun.* 1993;192:553–560.
11. Ichiki Y, Kitamura K, Kangawa K, et al. Distribution and characterization of immunoreactive adrenomedullin in human tissue and plasma. *FEBS Lett.* 1994;338:6–10.
12. Sakata J, Shimokubo T, Kitamura K, et al. Distribution and characterization of immunoreactive rat adrenomedullin in tissue and plasma. *FEBS Lett.* 1994;352:105–108.
13. Owji AA, Smith DM, Coppock HA, et al. An abundant and specific binding site for the novel vasodilator adrenomedullin in the rat. *Endocrinology.* 1995;136:2127–2134.
14. Kakishita M, Nishikimi T, Okano Y, et al. Increased plasma levels of adrenomedullin in patients with pulmonary hypertension. *Clin Sci.* 1999;96:33–39.
15. Yoshibayashi M, Kamiya T, Kitamura K, et al. Plasma levels of adrenomedullin in primary and secondary pulmonary hypertension in patients < 20 years of age. *Am J Cardiol.* 1997;79:1556–1558.
16. Horio T, Kohno M, Kano H, et al. Adrenomedullin as a novel antimigration factor of vascular smooth muscle cells. *Circ Res.* 1995;77:660–664.
17. Kano H, Kohno M, Yasunari K, et al. Adrenomedullin as a novel antiproliferative factor of vascular smooth muscle cells. *J Hypertens.* 1996;14:209–213.
18. Nagaya N, Satoh T, Nishikimi T, et al. Hemodynamic, renal, and hormonal effects of adrenomedullin infusion in patients with congestive heart failure. *Circulation.* 2000;101:498–503.
19. Nagaya N, Nishikimi T, Uematsu M, et al. Haemodynamic and hormonal effects of adrenomedullin in patients with pulmonary hypertension. *Heart.* 2000;84:653–658.
20. Walmrath D, Schneider T, Pilch J, et al. Aerosolized prostacyclin reduces pulmonary artery pressure and improves gas exchange in the adult respiratory distress syndrome (ARDS). *Lancet.* 1993;342:961–962.
21. Hoeper MM, Schwarze M, Ehlerding S, et al. Long-term treatment of primary pulmonary hypertension with aerosolized iloprost, a prostacyclin analogue. *N Engl J Med.* 2000;342:1866–1870.
22. Rich S, Seidlitz M, Dodin E, et al. The short-term effects of digoxin in patients with right ventricular dysfunction from pulmonary hypertension. *Chest.* 1998;114:787–792.
23. Miyamoto S, Nagaya N, Satoh T, et al. Clinical correlates and prognostic significance of six-minute walk test in patients with primary pulmonary

hypertension: comparison with cardiopulmonary exercise testing. *Am J Respir Crit Care Med*. 2000;161:487–492.
24. Ohta H, Tsuji T, Asai S, et al. A simple immunoradiometric assay for measuring the entire molecules of adrenomedullin in human plasma. *Clin Chim Acta*. 1999;287:131–143.
25. Lippton H, Chang JK, Hao Q, et al. Adrenomedullin dilates the pulmonary vascular bed in vivo. *J Appl Physiol*. 1994;76:2154–2156.
26. Heaton J, Lin B, Chang JK, et al. Pulmonary vasodilation to adrenomedullin: a novel peptide in humans. *Am J Physiol*. 1995;268:H2211–H2215.
27. Nossaman BD, Feng CJ, Kaye AD, et al. Pulmonary vasodilator responses to adrenomedullin are reduced by NOS inhibitors in rats but not in cats. *Am J Physiol*. 1996;270:L782–L789.
28. Ishizaka Y, Ishizaka Y, Tanaka M, et al. Adrenomedullin stimulates cyclic AMP formation in rat vascular smooth muscle cells. *Biochem Biophys Res Commun*. 1994;200:642–646.
29. Nakamura M, Yoshida H, Makita S, et al. Potent and long-lasting vasodilatory effects of adrenomedullin in humans: comparisons between normal subjects and patients with chronic heart failure. *Circulation*. 1997;95:1214–1221.
30. Nagaya N, Nishikimi T, Yoshihara F, et al. Cardiac adrenomedullin gene expression and peptide accumulation after acute myocardial infarction in rats. *Am J Physiol*. 2000;278:R1019–R1026.
31. Champion HC, Bivalacqua TJ, Toyoda K, et al. In vivo gene transfer of prepro-calcitonin gene-related peptide to the lung attenuates chronic hypoxia-induced pulmonary hypertension in the mouse. *Circulation*. 2000;101:931–937.
32. Ishiyama Y, Kitamura K, Ichiki Y, et al. Haemodynamic responses to rat adrenomedullin in anaesthetized spontaneously hypertensive rats. *Clin Exp Pharmacol Physiol*. 1995;22:614–618.
33. D'Alonzo GE, Gianotti LA, Pohil RL, et al. Comparison of progressive exercise performance of normal subjects and patients with primary pulmonary hypertension. *Chest*. 1987;92:57–62.
34. Wensel R, Opitz CF, Anker SD, et al. Assessment of survival in patients with primary pulmonary hypertension: importance of cardiopulmonary exercise testing. *Circulation*. 2002;106:319–324.
35. Anderson P, Saltin B. Maximal perfusion of skeletal muscle in man. *J Appl Physiol*. 1985;366:233–249.
36. Nagaya N, Okumura H, Uematsu M, et al. Repeated inhalation of adrenomedullin ameliorates pulmonary hypertension and survival in monocrotaline rats. *Am J Physiol Heart Circ Physiol*. 2005;285:H2125–H2131.
37. Skyler JS, Cefalu WT, Kourides IA, et al. Efficacy of inhaled human insulin in type 1 diabetes mellitus: a randomised proof-of-concept study. *Lancet*. 2001;357:331–335.

Adrenomedullin Gene Transfer Induces Therapeutic Angiogenesis in a Rabbit Model of Chronic Hind Limb Ischemia

Benefits of a Novel Nonviral Vector, Gelatin

Noriyuki Tokunaga, MD; Noritoshi Nagaya, MD; Mikiyasu Shirai, MD; Etsuro Tanaka, MD; Hatsue Ishibashi-Ueda, MD; Mariko Harada-Shiba, MD; Munetake Kanda, MD; Takefumi Ito, MD; Wataru Shimizu, MD; Yasuhiko Tabata, PhD; Masaaki Uematsu, MD; Kazuhiro Nishigami, MD; Shunji Sano, MD; Kenji Kangawa, PhD; Hidezo Mori, MD

Background—Earlier studies have shown that adrenomedullin (AM), a potent vasodilator peptide, has a variety of cardiovascular effects. However, whether AM has angiogenic potential remains unknown. This study investigated whether AM gene transfer induces therapeutic angiogenesis in chronic hind limb ischemia.

Methods and Results—Ischemia was induced in the hind limb of 21 Japanese White rabbits. Positively charged biodegradable gelatin was used to produce ionically linked DNA-gelatin complexes that could delay DNA degradation. Human AM DNA (naked AM group), AM DNA-gelatin complex (AM-gelatin group), or gelatin alone (control group) was injected into the ischemic thigh muscles. Four weeks after gene transfer, significant improvements in collateral formation and hind limb perfusion were observed in the naked AM group and AM-gelatin group compared with the control group (calf blood pressure ratio: 0.60±0.02, 0.72±0.03, 0.42±0.06, respectively). Interestingly, hind limb perfusion and capillary density of ischemic muscles were highest in the AM-gelatin group, which revealed the highest content of AM in the muscles among the three groups. As a result, necrosis of lower hind limb and thigh muscles was minimal in the AM-gelatin group.

Conclusions—AM gene transfer induced therapeutic angiogenesis in a rabbit model of chronic hind limb ischemia. Furthermore, the use of biodegradable gelatin as a nonviral vector augmented AM expression and thereby enhanced the therapeutic effects of AM gene transfer. Thus, gelatin-mediated AM gene transfer may be a new therapeutic strategy for the treatment of peripheral vascular diseases. **(*Circulation*. 2004;109:526-531.)**

Key Words: peripheral vascular disease ■ angiogenesis ■ gene therapy ■ ischemia

Adrenomedullin (AM) is a potent vasodilator peptide that was originally isolated from human pheochromocytoma.[1] AM and its receptor are expressed mainly in vascular endothelial cells and vascular smooth muscle cells.[2–4] AM not only induces vasorelaxation but also regulates growth and death of these vascular cells.[5–10] These findings suggest that AM plays an important role in maintaining vascular homeostasis in an autocrine and/or paracrine manner.

A recent study has shown that vascular abnormalities are present in homozygous AM knockout mice, suggesting that AM is indispensable for vascular morphogenesis.[11–13] More recently, AM has been shown to activate the PI3K Akt-dependent pathway in vascular endothelial cells, which is considered to regulate multiple critical steps in angiogenesis, including endothelial cell survival, proliferation, migration, and capillary-like structure formation.[7,14] These results raise the possibility that AM plays a role in modulating vasculogenesis and angiogenesis. However, whether AM induces therapeutic angiogenesis remains unknown.

Received May 20, 2003; revision received September 25, 2003; accepted September 26, 2003

From the Department of Cardiac Physiology, National Cardiovascular Center Research Institute, Osaka, Japan (N.T., M.S., M.K., H.M.); the Department of Cardiovascular Surgery, Okayama University Medical School, Okayama, Japan (N.T., S.S.); the Department of Regenerative Medicine and Tissue Engineering, National Cardiovascular Center Research Institute, Osaka, Japan (N.N., T.I.); the Department of Internal Medicine, National Cardiovascular Center, Osaka, Japan (N.N., W.S., K.N.); the Department of Physiology, the Research Center for Genetic Engineering and Cell Transplantation, Tokai University School of Medicine, Isehara, Japan (E.T.); the Department of Pathology, National Cardiovascular Center, Osaka, Japan (H.I.-U.); the Department of Biochemistry, National Cardiovascular Center Research Institute, Osaka, Japan (M.H.-S., K.K.); the Department of Biomaterials, Field of Tissue Engineering, Institute for Frontier Medical Sciences, Kyoto University, Kyoto, Japan (Y.T.); and the Cardiovascular Division, Kansai Rosai Hospital, Hyogo, Japan (M.U.)

Correspondence to Noritoshi Nagaya, MD, Department of Regenerative Medicine and Tissue Engineering or Hidezo Mori, MD, Department of Cardiac Physiology, National Cardiovascular Center Research Institute, 5-7-1 Fujishirodai, Suita, Osaka 565-8565, Japan. E-mail nagayann@hsp.ncvc.go.jp or hidemori@ri.ncvc.go.jp

Circulation is available at http://www.circulationaha.org

DOI: 10.1161/01.CIR.0000109700.81266.32

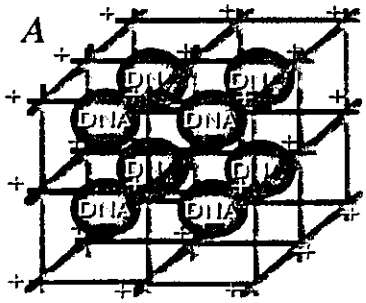

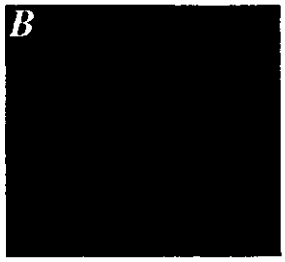

Figure 1. A, Schema of DNA-gelatin complex. Biodegradable gelatin can hold negatively charged plasmid DNA in its positively charged lattice structure. B, RITC-labeled AM DNA particles were incorporated into gelatin.

We prepared biodegradable gelatin that could hold negatively charged protein or plasmid DNA in its positively charged lattice structure.[15,16] Biodegradable gelatin has been widely used as a carrier of protein because of its capacity to delay protein degradation.[15] Similarly, ionically linked DNA-gelatin complexes can delay gene degradation.[16] These findings raise the possibility that gelatin may serve as a nonviral vector for gene therapy.

Thus, the purposes of this study were (1) to investigate whether AM gene transfer induces therapeutic angiogenesis in a rabbit model of chronic hind limb ischemia and (2) to examine whether the use of biodegradable gelatin as a vector augments AM expression and thereby enhances the therapeutic effects of AM gene transfer.

Methods

Animal Model

All protocols were performed in accordance with the guidelines of the Animal Care Ethics Committee of the National Cardiovascular Center Research Institute. Twenty-one male Japanese White rabbits (body weight, 2.9±0.1 kg; Japan Animal Co, Osaka, Japan) were used for physiological and morphological assessment. In addition, 30 rabbits were used for radioimmunoassay, immunohistochemical examination, and Western blot analysis. After anesthetization with pentobarbital sodium (30 to 35 mg/kg), a longitudinal incision was made in the left thigh, extending inferiorly from the inguinal ligament to a point just proximal to the patella. Hind limb ischemia was induced by ligation of the distal left external iliac artery and complete resection of the left femoral artery, as described previously.[17]

Construction of Plasmid DNA

To construct the expression vector for human AM, the *EcoRI-XhoI* fragment of the full-length human AM cDNA was ligated into the EcoRI-XhoI fragment of the pcDNA1.1-CMV expression plasmid (Invitrogen). To verify that the pcDNA1.1-CMV vector encoding AM cDNA produces a biologically active AM protein, the expression vector was transfected into 293 cells, and AM activity in the transfected cells was measured by high-performance liquid chromatography and radioimmunoassay. The pcDNA1.1-CMV vector encoding β-galactosidase (LacZ) cDNA was used as a control DNA.

Preparation of AM DNA-Gelatin Complex

Biodegradable gelatin was prepared from pig skin. The gelatin was characterized by a spheroid shape with a diameter of approximately 30 μm, water content of 95%, and an isoelectric point (pI) of 9 after swelling in water.[15,16] Gelatin can hold negatively charged protein or plasmid DNA in its positively charged lattice structure (Figure 1A). Dried gelatin (4 mg, pI 9) was added to human AM DNA solution (500 μg/100 μL) in phosphate-buffered saline, pH 7.4). After mixture of DNA and gelatin, DNA-gelatin complexes were incubated at 37°C for 2 hours.

To visualize incorporation of DNA into gelatin, AM plasmid DNA was labeled with rhodamine B isothiocyanate (RITC), as reported previously.[16] In brief, the coupling reaction of RITC to plasmid DNA was carried out by mixing the two substances in 0.2 mol/L sodium carbonate-buffered solution (pH 9.7), followed by gel filtration with a PD-10 column (Amersham-Pharmacia). RITC-labeled AM DNA was incorporated into positively charged gelatin (Figure 1B).

Study Protocol

Ten days after the induction of hind limb ischemia (day 10), AM DNA (naked AM group, n=7), AM DNA-gelatin complex (AM-gelatin group, n=7), or gelatin alone (control group, n=7) was administered intramuscularly into 3 different sites in the ischemic adductor muscle and 2 different sites in the semimembranous muscle. In addition, LacZ DNA-gelatin complex served as a control DNA (LacZ-gelatin group, n=5). The amount of plasmid was 500 μg (1 mL) and that of gelatin was 4 mg. Morphological and angiographic analyses and measurements of calf blood pressure and laser Doppler flow were performed 4 weeks after gene transfer (day 38). After completion of these measurements, the adductor, semimembranous, and gastrocnemius muscles were weighed in each hind limb.[18] The muscle weight ratio was calculated for each muscle as follows: muscle weight ratio=muscle weight in ischemic hind limb/muscle weight in nonischemic hind limb. Specimens of the adductor muscle of the ischemic hind limb were obtained for histological examination.

Measurement of Calf Blood Pressure

Calf blood pressure was measured on days 10 and 38 in both hind limbs with a Doppler flowmeter (Hayashi Denki Co, Ltd) and a 25-mm-wide cuff. The pulse of the posterior tibial artery was identified with the use of a Doppler probe, and the systolic blood pressure in both hind limbs was determined by standard techniques. The calf blood pressure ratio was defined for each rabbit as the ratio of systolic pressure of the ischemic hind limb to that of the normal hind limb.[17]

Laser Doppler Blood Perfusion Analysis

Blood flow of the ischemic hind limb was measured with the use of a laser Doppler blood perfusion image system (moorLDI, Moor Instruments) on day 38.

Angiographic Analysis

Development of collateral arteries was evaluated by angiography on days 0 and 38. A 4F catheter was placed in the left internal iliac artery through the common carotid artery, and 3 mL contrast medium (Iopamiron 300, SCHERING) was injected with an automated angiography injector at a rate of 2.5 mL/s. Quantitative angiographic analysis of collateral vessel development in the ischemic hind limb was performed with the use of a 5-mm grid overlay, as described previously.[17] The angiographic score was calculated for each film as the ratio of grid intersections crossed by opacified arteries divided by the total number of grid intersections in the ischemic medial thigh. The angiographic score was determined by 2 blinded observers.

Morphological and Histological Examination

The degree of lower hind limb necrosis and thigh muscle necrosis was macroscopically evaluated on graded morphological scales (grade 1 to 3) for peripheral tissue damage and muscle necrosis area of the adductor, semimembranous, and medial large muscles. Capillary density of the ischemic hind limb was evaluated by alkaline phosphatase staining, as reported previously.[17] A total of 10 different fields from three different sections were randomly selected, and the number of capillaries was counted under a ×40 objective. Capillary density was expressed as the mean number of capillaries per square millimeter. The number of myofibers in each field was also examined and the capillary/muscle fiber ratio calculated.

Radioimmunoassay for Human AM

Human AM production was examined 1, 2, and 4 weeks after gene transfer in the naked AM group, AM-gelatin group, and control group (n=5 each). The muscles were harvested for radioimmunoassay and immunohistochemical examination. Immunoreactive human AM level in rabbit muscles was determined by immunoradiometric assay with the use of a specific kit (Shionogi Co, Ltd).[19] Tissue content of vascular endothelial growth factor (VEGF) was examined by ELISA kit (R&D systems).

Immunohistochemistry for Human AM, Ki67 Antigen, and Phosphorylated Akt

Immunohistochemical studies were performed on formalin-fixed, paraffin-embedded 4-μm sections of ischemic thigh muscles 7 days after gene transfer. To elucidate AM expression after gene therapy, immunohistochemistry for human AM was performed with the use of a monoclonal antibody recognizing AM-(12-25) (1:100), as reported previously.[20] To evaluate the proliferative potential of AM, tissue sections were stained for Ki67, a marker for cell proliferation, with the use of monoclonal anti-Ki67 antibody (1:100) (DAKO). AM has recently been shown to promote proliferation of vascular endothelial cells at least in part through the PI3k/Akt pathway.[21] Thus, immunohistochemistry for phosphorylated Akt was performed with mouse monoclonal anti-phosphorylated Akt antibody (1:100) (Cell Signaling Technology).

Western Blot Analysis

To identify Akt phosphorylation in ischemic muscles after AM gene transfer, Western blotting was performed with the use of a commercially available kit (PhosphoPlus Akt [Ser473] Antibody Kit, Cell Signaling Technology). Ischemic muscles in the 3 groups were obtained 7 days after AM gene transfer. These samples were homogenized on ice in 0.1% Tween 20 homogenization buffer with a protease inhibitor (Complete, Roche). After centrifugation for 20 minutes at 4°C, the supernatant was used for Western blot analysis. The 50 μg of protein was transferred into sample buffer, loaded on 7.5% SDS-polyacrylamide gel, and blotted onto nitrocellulose membrane through the use of a wet blotting system. After blocking for 60 minutes, the membranes were incubated with primary antibodies (1:500) at 4°C overnight. The membranes were then incubated with secondary antibodies, which were conjugated with horseradish peroxidase (Cell Signaling Technology), at a final dilution of 1:2000. Signals were detected through the use of LumiGLO chemiluminescence reagents (Cell Signaling Technology).

Statistical Analysis

All results are expressed as mean±SEM. Statistical significance was evaluated by 1-way ANOVA followed by Fisher's analysis, Scheffe's F analysis, or Kruskal-Wallis test. A value of $P<0.05$ was considered statistically significant.

Results

Physiological and Morphological Assessment

Complete resection of the left femoral artery resulted in a similar decrease in calf blood pressure ratio among the 3 groups before the initiation of therapy (day 10) (Figure 2A). However, the calf blood pressure ratio on day 38 was highest in the AM-gelatin groups, followed by the naked AM group and subsequently the control group. The laser Doppler flow in hind limb was highest in the AM-gelatin group, followed by the naked AM group and the control group (Figure 2B). The calf blood pressure ratio and laser Doppler flow 4 weeks after gene transfer did not significantly differ between the control group and Lac Z-gelatin group. Lower hind limb necrosis was minimal in the AM-gelatin group, followed by the naked AM group and the control group (Figure 2C). Thigh muscle necrosis was also minimal in the AM-gelatin group. Similarly, the muscle weight ratio (ischemic/normal) on day 38 was highest in the AM-gelatin group (Table). Neither mean arterial pressure nor heart rate significantly differed among the 3 groups.

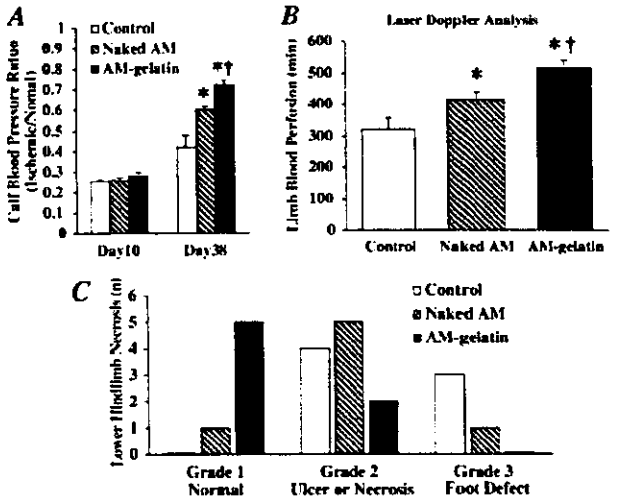

Figure 2. A, Calf blood pressure ratio (ischemic/normal hind limb) before (on day 10) and after (on day 38) gene transfer. B, Measurement of laser Doppler flow on day 38. Data are mean±SEM. *$P<0.05$ vs control group; †$P<0.05$ vs naked AM group. C, Number of cases of each grade of lower hind limb necrosis on day 38. Lower hind limb necrosis was minimal in the AM-gelatin group. Number of necrosis or foot defect is statistically significant among the 3 groups ($P<0.05$ by Kruskal-Wallis test).

Angiographic Analysis

Angiograms 4 weeks after gene transfer (day 38) showed the development of collateral arteries in the naked AM and

Physiological Characteristics

	Control	Naked AM	AM-Gelatin
No. of rabbits	7	7	7
Body weight, kg	2.46±0.06	2.65±0.10	3.16±0.09
MAP, mm Hg	112±3	114±3	116±2
HR, beats/min	269±12	253±5	262±7
Muscle weight ratio	0.71±0.03	0.84±0.02*	0.95±0.02*†

MAP indicates mean arterial pressure; HR, heart rate; and muscle weight ratio, ratio of muscle weight in ischemic hind limb to that in nonischemic hind limb. Data are mean±SEM.

*$P<0.01$ vs control group; †$P<0.05$ vs naked AM group.

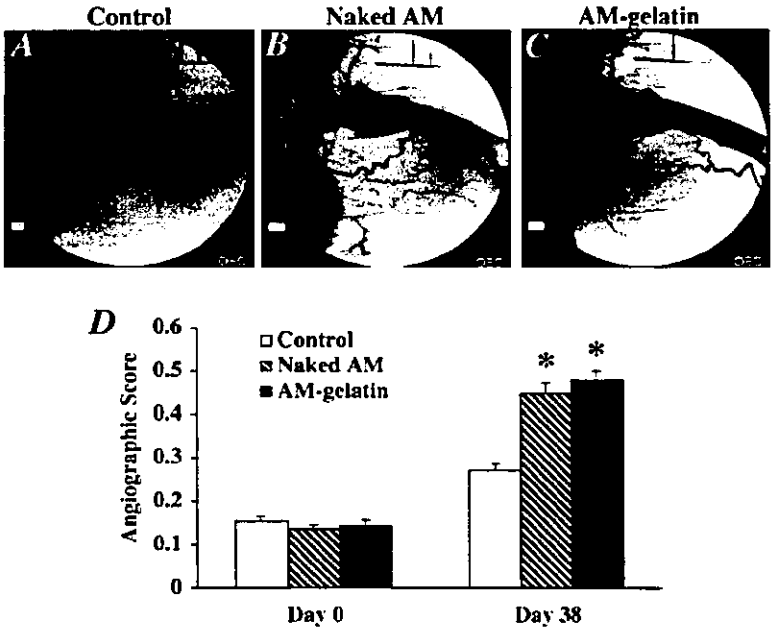

Figure 3. Representative angiograms of control group (A), naked AM group (B), and AM-gelatin group (C) on day 38. Collateral arteries were well developed in the naked AM and AM-gelatin groups. D, Angiographic score on days 0 and 38 in each group. Angiographic score on day 38 was significantly higher in the naked AM and AM-gelatin groups than in the control group. Data are mean ± SEM. *$P<0.001$ versus control group.

AM-gelatin groups compared with that in the control group (Figure 3, A through C). Quantitative analysis of collateral vessels demonstrated that the angiographic score in both the naked AM and AM-gelatin groups was significantly higher than that in the control group (Figure 3D). Angiographic score did not significantly differ between the control group and Lac Z-gelatin group.

To examine the development of collateral vessels in an earlier stage, other rabbits (n=4 each) were examined 2 weeks after gene transfer (day 24). Angiograms showed significant collateral development in the naked AM and AM-gelatin groups compared with that in the control group.

Histological Examination

Alkaline phosphatase staining of ischemic hind limb muscle showed marked augmentation of neovascularization in both the naked AM and AM-gelatin groups compared with the control group (Figure 4, A through C). Quantitative analysis demonstrated that capillary density of the ischemic adductor muscle was highest in the AM-gelatin group (Figure 4D). Analysis of the capillary muscle fiber ratio yielded similar results. Seven days after gene transfer, intense immunostaining for Ki67 was observed in vascular endothelial cells of the naked AM and the AM-gelatin groups (Figure 4, E through G).

AM Expression and Akt Phosphorylation After Gene Transfer

Seven days after gene transfer, modest immunostaining for human AM was observed in the naked AM group, whereas AM immunoreactivity was intense surrounding the gelatin in the AM-gelatin group (Figure 5, A through C). Tissue content of human AM was significantly increased both in the naked AM and the AM-gelatin groups 7 days after gene transfer (Figure 5D). The AM level in the AM-gelatin group was significantly higher that in the naked AM group. Two weeks after gene transfer, AM overexpression was observed only in the AM-gelatin group. The expression of endogenous VEGF and its receptors (Flt-1 and Flk-1) did not differ among the 3 groups (data not shown). Western blot analysis revealed that phosphorylated Akt in ischemic muscles was increased in both the naked AM and AM-gelatin groups 7 days after gene transfer (Figure 5E). Intense immunostaining for phosphory-

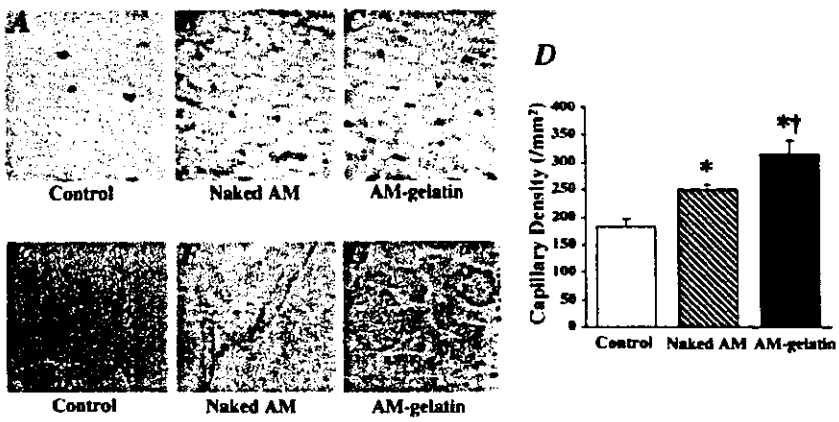

Figure 4. A through C, Representative examples of alkaline phosphatase staining in ischemic hind limb muscles. Magnification ×200. D, Quantitative analysis of capillary density in ischemic hind limb muscles. Data are mean ± SEM. *$P<0.05$ vs control group; †$P<0.05$ vs naked AM group. E through G, Immunohistochemical analysis of Ki67 antigen, a marker for cell proliferation. Magnification ×400.

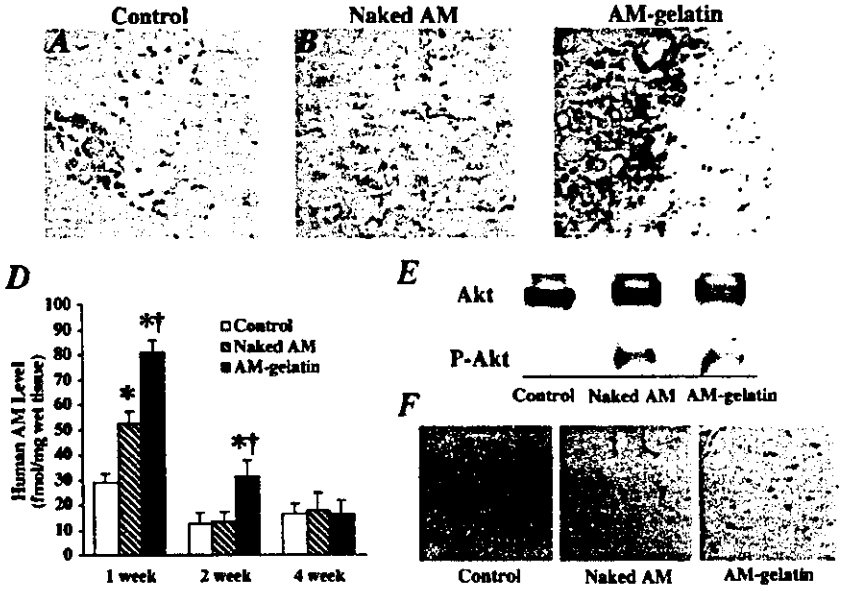

Figure 5. A through C, Immunohistochemistry for human AM 7 days after gene transfer. Intense immunostaining was observed surrounding gelatin in the AM-gelatin group. Magnification ×200. D, Time course of AM production in ischemic muscles after gene transfer. Data are mean±SEM. *$P<0.01$ vs control group; †$P<0.01$ vs naked AM group. E, Western blot analysis for Akt phosphorylation in muscles. F, Immunohistochemical staining for phosphorylated Akt 7 days after gene transfer. Phosphorylated Akt was distributed at least in endothelial cells. Magnification ×400.

lated Akt was observed at least in endothelial cells of the Naked AM and the AM-gelatin groups (Figure 5F).

Discussion

We demonstrated that (1) AM gene transfer induced hemodynamic and angiographic improvements in association with an increase in capillary density in a rabbit model of chronic hind limb ischemia. We also demonstrated that (2) administration of AM DNA-gelatin complexes markedly augmented AM expression and thereby enhanced the therapeutic effects of AM gene transfer.

AM has a variety of effects on the vasculature that include vasodilation,[1,5-7] inhibition of endothelial cell apoptosis,[8,9] and regulation of smooth muscle cell proliferation.[10] However, whether AM has angiogenic potential has remained unknown. In the present study, intramuscular administration of naked AM DNA augmented AM production in skeletal muscles, as indicated by increased tissue content and significant immunostaining of AM. As a result, AM gene transfer increased hind limb perfusion and ameliorated lower hind limb and thigh muscle necrosis in a rabbit model of hind limb ischemia. AM gene transfer may protect the ischemic hind limb partly by improving the blood flow in the ischemic hind limb because AM is originally identified as a potent vasodilating peptide.[1] Nevertheless, angiographic collateral development and high capillary density were observed in ischemic muscles after AM gene transfer. Ki67, a marker for cell proliferation, was detected in endothelial cells of microvessels after AM gene transfer. These results suggest that AM overproduction resulting from gene transfer may induce angiogenesis in a rabbit model of hind limb ischemia. Recent studies using AM gene knockout mice have shown that AM is essential for development of the vasculature during embryogenesis.[11-13] These studies support our results that AM may be an angiogenic factor. VEGF is known to induce angiogenesis and to regulate endothelial cell survival through the phosphatidylinositol 3-kinase (PI3K) Akt pathway.[22] Thus, the PI3K/Akt pathway is considered to regulate multiple critical steps in angiogenesis, including endothelial cell survival, proliferation, migration, and capillary-like structure formation.[14] A recent study has reported that AM promotes proliferation and migration of human umbilical vein endothelial cells at least in part through the PI3K/Akt pathway.[21] The present study demonstrated that phosphorylated Akt is increased at least in endothelial cells after AM gene transfer. AM gene transfer did not influence endogenous VEGF and its receptors. Taken together, it is interesting to speculate that AM may directly induce angiogenesis through the PI3K/Akt pathway.

In the present study, we used positively charged biodegradable gelatin as a nonviral vector. We have shown that basic fibroblast growth factor (bFGF) is ionically linked with gelatin, which enhances the angiogenic effects of bFGF by delaying protein degradation.[15] Thus, biodegradable gelatin has been used as a carrier of protein. However, little information is available regarding the therapeutic potential of gelatin as a nonviral vector for gene transfer. In the present study, we demonstrated that RITC-labeled AM DNA was incorporated into positively charged gelatin. In addition, intramuscular administration of AM DNA-gelatin complexes strongly enhanced AM production compared with that of naked AM DNA. These results suggest that biodegradable gelatin may serve as a vector for gene transfer. In fact, AM DNA-gelatin complexes induced more potent angiogenic effects in a rabbit model of hind limb ischemia than naked AM DNA, as evidenced by significant increases in histological capillary density, calf blood pressure ratio, laser Doppler flow, and muscle weight ratio and a decrease in necrosis of lower hind limb and thigh muscles. These results suggest that the use of biodegradable gelatin as a nonviral vector augments AM expression and enhances AM-induced angiogenic effects. The angiogenic effects of AM-gelatin complexes were comparable to those of bFGF-gelatin complexes (data not shown). AM DNA-gelatin complexes were distributed mainly in connective tissues. We have recently demonstrated that gelatin-DNA complex is readily phagocytosed by mac-

rophages, monocytes, endothelial progenitor cells, and so on, resulting in gene expression within these phagocytes.[23,24] These findings raise the possibility that AM secreted from these cells acts on muscles in a paracrine fashion. Unlike AM production in the naked AM group, AM overexpression in the AM-gelatin group lasted for longer than 2 weeks. Thus, it is interesting to speculate that delaying gene degradation by gelatin may be responsible for the highly efficient gene transfer.

Currently, a highly efficient and safe gene delivery system is needed for gene therapy in humans. The present study demonstrated that the use of gelatin, which is considered to be less biohazardous than viral vectors, enhanced the angiogenic potential of AM DNA. Thus, gelatin-mediated AM gene transfer may be a new therapeutic strategy for the treatment of severe peripheral vascular diseases. However, the initial success of gelatin-mediated AM gene therapy reported here should be confirmed by long-term experiments, and extensive toxicity studies in animals are needed before clinical trials.

Study Limitation

First, histological capillary density, calf blood pressure ratio, and laser Doppler flow were significantly higher in the AM-gelatin group than in the naked AM group. However, the angiographic score did not significantly differ between the two. This discrepancy raises the possibility that conventional angiography may have insufficient resolution to fully visualize the angiogenic microvessels. Second, human AM level was slightly elevated in the control group. This implies that the anti-human AM antibody used in this radioimmunoassay had some cross-reactivity with endogenous rabbit AM. Nevertheless, human AM level in the muscles was highest in the AM-gelatin group within 2 weeks after gene transfer. These results suggest that AM DNA-gelatin complexes induces potent and long-lasting AM production.

Conclusions

Intramuscular administration of AM DNA induced therapeutic angiogenesis in a rabbit model of chronic hind limb ischemia. Furthermore, the use of biodegradable gelatin as a nonviral vector augmented AM expression and thereby enhanced the therapeutic effects of AM gene transfer. Thus, gelatin-mediated AM gene transfer may be a new therapeutic strategy for the treatment of peripheral vascular diseases.

Acknowledgments

This work was supported by a grant from the Japan Cardiovascular Research Foundation, HLSRG-RAMT-nano-001 and -RHGTEFB-genome-005, RGCD13C-1 from MHLW, grants from NEDO, a Grant-in-Aid for Scientific research from MECSST (13470154 and13877114), and the Promotion of Fundamental Studies in Health Science of the Organization for Pharmaceutical Safety and Research (OPSR) of Japan.

References

1. Kitamura K, Kangawa K, Kawamoto M, et al. Adrenomedullin: a novel hypotensive peptide isolated from human pheochromocytoma. *Biochem Biophys Res Commun*. 1993;192:553–560.
2. Sugo S, Minamino N, Kangawa K, et al. Endothelial cells actively synthesize and secrete adrenomedullin. *Biochem Biophys Res Commun*. 1994;201:1160–1166.
3. Sugo S, Minamino N, Shoji H, et al. Production and secretion of adrenomedullin from vascular smooth muscle cells: augmented production by tumor necrosis factor-alpha. *Biochem Biophys Res Commun*. 1994;203:719–726.
4. Kato J, Kitamura K, Kangawa K, et al. Receptors for adrenomedullin in human vascular endothelial cells. *Eur J Pharmacol*. 1995;289:383–385.
5. Shimekake Y, Nagata K, Ohta S, et al. Adrenomedullin stimulates two signal transduction pathways, cAMP accumulation and Ca^{2+} mobilization, in bovine aortic endothelial cells. *J Biol Chem*. 1995;270:4412–4417.
6. Nagaya N, Satoh T, Nishikimi T, et al. Hemodynamic, renal, and hormonal effects of adrenomedullin infusion in patients with congestive heart failure. *Circulation*. 2000;101:498–503.
7. Nishimatsu H, Suzuki E, Nagata D, et al. Adrenomedullin induces endothelium-dependent vasorelaxation via the phosphatidylinositol 3-kinase/Akt-dependent pathway in rat aorta. *Circ Res*. 2001;89:63–70.
8. Kato H, Shichiri M, Marumo F, et al. Adrenomedullin as an autocrine/paracrine apoptosis survival factor for rat endothelial cells. *Endocrinology*. 1997;138:2615–2620.
9. Sata M, Kakoki M, Nagata D, et al. Adrenomedullin and nitric oxide inhibit human endothelial cell apoptosis via a cyclic GMP-independent mechanism. *Hypertension*. 2000;36:83–88.
10. Kano H, Kohno M, Yasunari K, et al. Adrenomedullin as a novel antiproliferative factor of vascular smooth muscle cells. *J Hypertens*. 1996;14:209–213.
11. Shindo T, Kurihara Y, Nishimatsu H, et al. Vascular abnormalities and elevated blood pressure in mice lacking adrenomedullin gene. *Circulation*. 2001;104:1964–1971.
12. Caron KM, Smithies O. Extreme hydrops fetalis and cardiovascular abnormalities in mice lacking a functional adrenomedullin gene. *Proc Natl Acad Sci U S A*. 2001;98:615–619.
13. Imai Y, Shindo T, Maemura K, et al. Evidence for the physiological and pathological roles of adrenomedullin from genetic engineering in mice. *Ann N Y Acad Sci*. 2001;947:26–34.
14. Shiojima I, Walsh K. Role of Akt signaling in vascular homeostasis and angiogenesis. *Circ Res*. 2002;90:1243–1250.
15. Tabata Y, Hijikata S, Muniruzzaman M, et al. Neovascularization effect of biodegradable gelatin microspheres incorporating basic fibroblast growth factor. *J Biomater Sci Polym Ed*. 1999;10:79–94.
16. Fukunaka Y, Iwanaga K, Morimoto K, et al. Controlled release of plasmid DNA from cationized gelatin hydrogels based on hydrogel degradation. *J Control Release*. 2002;80:333–343.
17. Takeshita S, Zheng LP, Brogi E, et al. Therapeutic angiogenesis: a single intraarterial bolus of vascular endothelial growth factor augments revascularization in a rabbit ischemic hindlimb model. *J Clin Invest*. 1994;93:662–670.
18. Van Belle E, Witzenbichler B, Chen D, et al. Potentiated angiogenic effect of scatter factor/hepatocyte growth factor via induction of vascular endothelial growth factor. *Circulation*. 1998;97:381–390.
19. Ohta H, Tsuji T, Asai S, et al. A simple immunoradiometric assay for measuring the entire molecules of adrenomedullin in human plasma. *Clin Chim Acta*. 1999;287:B131–B143.
20. Nagaya N, Nishikimi T, Yoshihara F, et al. Cardiac adrenomedullin gene expression and peptide accumulation after acute myocardial infarction in rats. *Am J Physiol Regul Integr Comp Physiol*. 2000;278:R1019–R1026.
21. Miyashita K, Itoh H, Sawada N, et al. Adrenomedullin promotes proliferation and migration of cultured endothelial cells. *Hypertens Res*. 2003;26:S93–S98.
22. Jiang BH, Zheng JZ, Aoki M, et al. Phosphatidylinositol 3-kinase signaling mediates angiogenesis and expression of vascular endothelial growth factor in endothelial cells. *Proc Natl Acad Sci U S A*. 2000;97:1749–1753.
23. Tabata Y, Ikada Y. Macrophage activation through phagocytosis of muramyl dipeptide encapsulated in gelatin microspheres. *J Pharm Pharmacol*. 1987;39:698–704.
24. Nagaya N, Kangawa K, Kanda M, et al. Hybrid cell-gene therapy for pulmonary hypertension based on phagocytosing action of endothelial progenitor cells. *Circulation*. 2003;108:889–895.

Available online at www.sciencedirect.com
SCIENCE DIRECT
Neurochemistry International 44 (2004) 497–503
NEUROCHEMISTRY International
www.elsevier.com/locate/neuint

Simultaneous monitoring of acetylcholine and catecholamine release in the in vivo rat adrenal medulla

Tsuyoshi Akiyama [a,*], Toji Yamazaki [a], Hidezo Mori [a], Kenji Sunagawa [b]

[a] *Department of Cardiac Physiology, National Cardiovascular Center Research Institute, 5-7-1 Fujishiro-dai, Suita, Osaka 565-8565, Japan*
[b] *Department of Cardiovascular Dynamics, National Cardiovascular Center Research Institute, Suita, Osaka 565-8565, Japan*

Received 20 May 2003; accepted 3 September 2003

Abstract

To simultaneously monitor acetylcholine release from pre-ganglionic adrenal sympathetic nerve endings and catecholamine release from post-ganglionic adrenal chromaffin cells in the in vivo state, we applied microdialysis technique to anesthetized rats. Dialysis probe was implanted in the left adrenal medulla and perfused with Ringer's solution containing neostigmine (a cholinesterase inhibitor). After transection of splanchnic nerves, we electrically stimulated splanchnic nerves or locally administered acetylcholine through dialysis probes for 2 min and investigated dialysate acetylcholine, choline, norepinephrine and epinephrine responses. Acetylcholine was not detected in dialysate before nerve stimulation, but substantial acetylcholine was detected by nerve stimulation. In contrast, choline was detected in dialysate before stimulation, and dialysate choline concentration did not change with repetitive nerve stimulation. The estimated interstitial acetylcholine levels and dialysate catecholamine responses were almost identical between exogenous acetylcholine (10 μM) and nerve stimulation (2 Hz). Dialysate acetylcholine, norepinephrine and epinephrine responses were correlated with the frequencies of electrical nerve stimulation, and dialysate norepinephrine and epinephrine responses were quantitatively correlated with dialysate acetylcholine responses. Neither hexamethonium (a nicotinic receptor antagonist) nor atropine (a muscarinic receptor antagonist) affected the dialysate acetylcholine response to nerve stimulation. Microdialysis technique made it possible to simultaneously assess activities of pre-ganglionic adrenal sympathetic nerves and post-ganglionic adrenal chromaffin cells in the in vivo state and provided quantitative information about input–output relationship in the adrenal medulla.

Keywords: Anesthetized rats; Microdialysis; Choline; Norepinephrine; Epinephrine

1. Introduction

Although acetylcholine is one of major neurotransmitters in the peripheral autonomic nervous system as well as central nervous system (Collier, 1977; Fibiger, 1991; Calabresi et al., 2000), it has been difficult to measure endogenous acetylcholine in the in vivo state since acetylcholine released from nerve endings is rapidly degraded by tissue acetylcholinesterase (Taylor and Brown, 1998). Recently, microdialysis technique with improved measurement has made it possible to monitor low levels of acetylcholine in the in vivo central nervous system. In the peripheral autonomic nervous system, we have measured acetylcholine release from post-ganglionic parasympathetic nerve endings using microdialysis technique (Akiyama et al., 1994; Akiyama and Yamazaki, 2000, 2001; Kawada et al., 2001). Little information is, however, available on acetylcholine release from pre-ganglionic autonomic nerve endings in the in vivo state. The assessment of pre-ganglionic autonomic nerve activities is important for understanding the autonomic ganglionic transmission under physiological and pathophysiological conditions.

Adrenal medulla is one candidate suitable for investigating acetylcholine release from pre-ganglionic autonomic nerve endings (Holman et al., 1994). Compared to autonomic ganglia, adrenal gland is solid and suited to microdialysis probe implantation. Furthermore, microdialysis technique in the adrenal medulla provides a distinct advantage to monitor catecholamine release from adrenal medulla following acetylcholine release. Thus, we consider it possible to simultaneously assess pre- and post-ganglionic sympathetic nerve activities by monitoring acetylcholine and catecholamine release in the adrenal medulla.

In the present study, we applied the microdialysis technique to the adrenal medulla of anesthetized rats and tested the suitability of microdialysis technique to simultaneously

* Corresponding author. Tel.: +81-6-6833-5012x2380; fax: +81-6-6872-8092.
E-mail address: takiyama@ri.ncvc.go.jp (T. Akiyama).

0197-0186/$ – see front matter © 2003 Elsevier Ltd. All rights reserved.
doi:10.1016/j.neuint.2003.09.001

monitor acetylcholine and catecholamine release from adrenal medulla.

2. Materials and methods

2.1. Animal preparation

The investigation conforms with the *Guide for the Care and Use of Laboratory Animals* published by the US National Institutes of Health (NIH Publication No. 85-23, revised 1996). Adult male Wistar rats weighing 390–460 g were anesthetized with pentobarbital sodium (50–55 mg/kg i.p.). The rats were ventilated with a constant-volume respirator using room air mixed with oxygen. The left femoral artery and vein were cannulated for monitoring arterial blood pressure and administration of anesthetic, respectively. The level of anesthesia was maintained with a continuous intravenous infusion of pentobarbital sodium (15–25 mg/(kg h) i.v.). Electrocardiogram was monitored for recording heart rate. A thermostatic heating pad was used to keep the esophageal temperature within a range of 37–38 °C. With the animal in the lateral position, the left adrenal gland and left splanchnic nerve were exposed by a subcostal flank incision, and the left splanchnic nerve was transected. In protocols requiring nerve stimulation, shielded bipolar stainless steel electrodes were applied to the distal end of the nerve, which was then stimulated with a digital stimulator (SEN-7203, Nihon Kohden, Japan) with a rectangular pulse (10 V and 1 ms in duration).

2.2. Dialysis technique

The materials of the dialysis probe were the same as those used in our previous dialysis experiments (Akiyama et al., 2003). Briefly, each end of the dialysis fiber (0.31 mm o.d., and 0.20 mm i.d.; PAN-1200 50,000 mol. wt. cutoff, Asahi Chemical, Japan) was inserted into the polyethylene tube (25 cm length, 0.50 mm o.d., and 0.20 mm i.d.; SP-8) and glued. The length of the dialysis fiber exposed was 3 mm. At perfusion speed of 10 μl/min, in vitro recovery rates of acetylcholine, choline, norepinephrine, and epinephrine were (%): 3.08 ± 0.04, 2.93 ± 0.10, 2.09 ± 0.03, and 2.16 ± 0.03, respectively (number of dialysis probes: 3).

The dialysis probe was implanted in the medulla of the left adrenal gland and perfused with Ringer's solution containing the cholinesterase inhibitor, neostigmine (10 μM) at a speed of 10 μl/min using a microinjection pump (CMA/100, Carnegie Medicin, Sweden). Ringer's solution consisted of (in mM) 147.0 NaCl, 4.0 KCl, 2.25 $CaCl_2$. All pharmacological agents tested were locally administered by perfusion through the dialysis probe after being dissolved in Ringer's solution. One sampling period was 2 min (one sample volume = 20 μl). We started the protocols followed by a stabilization period of 3–4 h. Catecholamine release was evoked by 2 min-local administration of acetylcholine or 2 min-electrical stimulation of left splanchnic nerves. In protocols requiring repeated nerve stimulation, electrical stimulation was performed at 30 min-intervals. Taking the dead space volume into account, we continuously collected three dialysate samples per pharmacological or electrical stimulation: one before, one during, and one after stimulation. We subtracted the dialysate acetylcholine, norepinephrine, or epinephrine contents in control from those during stimulation, and expressed these values as indices of dialysate acetylcholine, norepinephrine or epinephrine response to stimulation.

Half of the dialysate sample was injected into high-performance liquid chromatography for the measurement of acetylcholine and choline (Akiyama et al., 1994), and the remaining half was injected into another high-performance liquid chromatography for the measurement of norepinephrine and epinephrine (Akiyama et al., 1991).

2.3. Experimental protocols

2.3.1. Protocol 1

We repeated stimulations of splanchnic nerves at 2 and 4 Hz twice and examined dialysate acetylcholine, choline and catecholamine responses to nerve stimulation and their reproducibility in five rats.

2.3.2. Protocol 2

To compare the estimated interstitial acetylcholine levels between administration of acetylcholine and nerve stimulation, we locally administered acetylcholine (10 μM) in five rats and stimulated splanchnic nerves at 2 Hz in five other rats. The concentration of exogenous acetylcholine was determined to obtain a similar dialysate catecholamine response to nerve stimulation at 2 Hz.

2.3.3. Protocol 3

We raised stepwise the frequency of nerve stimulation from 2 to 4, 10, 20 Hz and examined dialysate acetylcholine and catecholamine responses in five rats. In addition, to examine the input–output relationship in the adrenal medulla, we analyzed the relationship between dialysate acetylcholine and catecholamine responses of five rats.

2.3.4. Protocol 4

We examined the effects of cholinergic receptor antagonists on dialysate acetylcholine and catecholamine responses. Nerve stimulations at 2 and 4 Hz were performed before and after 30 min-local administration of cholinergic receptor antagonists. We tested the nicotinic receptor antagonist, hexamethonium bromide (1 mM) in five rats or the muscarinic receptor antagonist, atropine sulfate (10 μM) in five other rats.

2.4. Statistical methods

To examine the effect of nerve stimulation and pharmacological agents, we analyzed heart rate and mean

arterial pressure, and dialysate acetylcholine, choline, norepinephrine and epinephrine responses, using one- or two-way analysis of variance with repeated measures. When statistical significance was detected, the Newman–Keuls test was applied (Winer, 1971). Statistical significance was defined as $P < 0.05$. Values are presented as mean ± S.E.

3. Results

The experiments were carried in anesthetized rats and had been performed in the presence of neostigmine. Local administration of pharmacological agents did not influence heart rate or mean arterial pressure in any of the protocols. In protocol 3 ($n = 5$), nerve stimulation at 2 Hz decreased heart rate from 420 ± 8 to 397 ± 8 beats/min ($P < 0.05$) and increased mean arterial pressure from 125 ± 4 to 136 ± 3 mmHg ($P < 0.05$). Heart rate and mean arterial pressure recovered after cessation of stimulation. Nerve stimulation at 4, 10 and 20 Hz decreased heart rate to 396±9, 393±7 and 392 ± 9 beats/min, respectively, and increased mean arterial pressure to 134±3, 141±3, and 142±3 mmHg, respectively. In the other protocols, nerve stimulation at 2 or 4 Hz evoked the same responses of heart rate and mean arterial pressure.

3.1. Dialysate acetylcholine and catecholamine

3.1.1. Protocol 1

As shown in the *upper panel* of Fig. 1 ($n = 5$), acetylcholine was not detected in dialysate before nerve stimulation, but substantial acetylcholine was detected in dialysate by nerve stimulation. In contrast, choline, norepinephrine, and epinephrine were detected in dialysate before stimulation. Dialysate choline concentration did not change with repetitive nerve stimulation. Dialysate norepinephrine and epinephrine concentrations increased with nerve stimulation. Stimulation at the same frequency elicited almost identical responses on repetition.

3.1.2. Protocol 2

Using in vitro recovery rate of acetylcholine (3.08%), the estimated interstitial acetylcholine levels were 308 nM in acetylcholine infusion (10 μM, $n = 5$) and 276 ± 15 nM in nerve stimulation (2 Hz, $n = 5$; Fig. 1, *lower panel*). There was no statistical difference in the estimated interstitial acetylcholine levels and dialysate catecholamine responses between the two groups.

3.1.3. Protocol 3

When the frequency of nerve stimulation was increased from 2 to 20 Hz, dialysate acetylcholine, norepinephrine and epinephrine responses were enhanced ($n = 5$; Fig. 2, *upper panel*). We plotted the relationship between dialysate catecholamine response (ordinate) and dialysate acetylcholine response (abscissa) of five rats (Fig. 2, *lower panel*). Dialysate norepinephrine and epinephrine responses correlated with dialysate acetylcholine responses.

3.1.4. Protocol 4

At both 2 and 4 Hz of nerve stimulation, hexamethonium suppressed dialysate norepinephrine and epinephrine responses, but did not affect acetylcholine response ($n = 5$; Fig. 3, *upper panel*). Atropine suppressed epinephrine response at both 2 and 4 Hz of nerve stimulation, but did not affect norepinephrine and acetylcholine responses ($n = 5$; Fig. 3, *lower panel*).

4. Discussion

By now, simultaneous monitoring of adrenal acetylcholine and catecholamine release has been limited to only a few studies using perfused adrenal gland. Collier et al. (1984) measured endogenous acetylcholine and catecholamine effluxes from perfused cat adrenal gland. O'Farrell et al. (1997) preloaded bovine adrenal glands with [^{3}H]-choline and measured the subsequent efflux of [^{3}H]-labelled compound as an index of acetylcholine release and catecholamine efflux. In the present in vivo study, dialysate acetylcholine and catecholamine responses served as indices of acetylcholine release from splanchnic nerve endings and catecholamine release from adrenal medulla, respectively. This simultaneous monitoring implies quantitative measurement of pre- and post-ganglionic neurotransmitter release at the adrenal medulla.

4.1. Source of dialysate acetylcholine

The stimulation of splanchnic nerve induced acetylcholine release from pre-ganglionic nerve endings and increased dialysate acetylcholine concentration. It has been demonstrated that adrenal gland receives parasympathetic efferent and afferent innervation (Coupland et al., 1989; Niijima, 1992; Parker et al., 1993). Branches of parasympathetic efferent nerves conduct through celiac nerves, celiac ganglion and splanchnic nerves to adrenal nerves (Niijima, 1992). In the present study, we electrically stimulated the portion just distal to the sympathetic chain and proximal to the celiac ganglion. This portion does not contain branches of parasympathetic efferent nerves. After transection of splanchnic nerves, basal dialysate acetylcholine was less than the detection limit of high performance liquid chromatography (10 fmol), and substantial acetylcholine was detected in dialysate during the stimulation of this portion. Thus, most of the detected acetylcholine in dialysate derives from pre-ganglionic sympathetic nerve endings.

4.2. Interstitial choline levels in the adrenal medulla

Under physiological conditions, there is enough acetylcholinesterase activity in splanchnic nerve endings, chromaffin cells, and interstitial cells (Coupland, 1965; Palkama, 1967; Lewis and Shute, 1969; Somogyi et al., 1975). Released acetylcholine is degraded to choline and acetate by

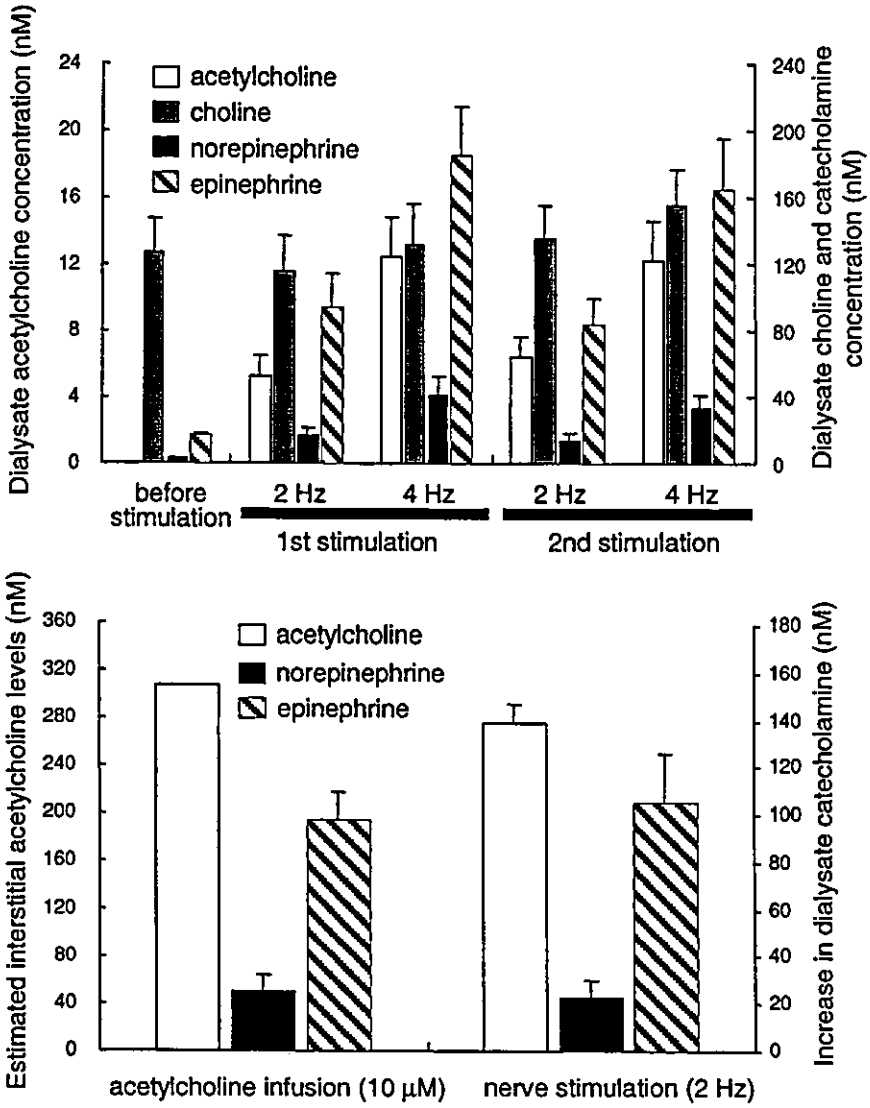

Fig. 1. (*Upper panel*) Acetylcholine was not detected in dialysate before nerve stimulation, but substantial acetylcholine was detected in dialysate by nerve stimulation (5 ± 1 nM at 2 Hz and 12 ± 2 nM at 4 Hz). Dialysate choline concentration did not change with nerve stimulation. Dialysate norepinephrine and epinephrine concentrations increased with nerve stimulation (17 ± 5 and 94 ± 20 nM at 2 Hz, respectively, and 41 ± 12 and 185 ± 29 nM at 4 Hz, respectively). Stimulation at the same frequency elicited almost identical responses on repetition, $n = 5$. Values are mean ± S.E. (*Lower panel*) There was no statistical difference in the estimated interstitial acetylcholine levels and dialysate catecholamine responses between acetylcholine infusion (10 μM, $n = 5$) and nerve stimulation (2 Hz, $n = 5$). Values are mean ± S.E.

acetylcholinesterase. Interstitial choline is carried into the nerve endings through neuronal transporters and used as a precursor for synthesis of acetylcholine (Taylor and Brown, 1998). In in vitro perfused experiments, continuous administration of choline sustains the synthesis and release of acetylcholine from nerve endings. In the present study, the concentration of dialysate choline was more than 10 times that of dialysate acetylcholine during nerve stimulation, and repetitive acetylcholine release did not induce a decrease in dialysate choline concentration. Moreover, nerve stimulation elicited almost identical responses of dialysate acetylcholine on repetition. These results indicate that repetitive acetylcholine release did not decrease interstitial choline levels and did not affect release of acetylcholine. Thus, under in vivo conditions, adrenal interstitial choline levels may be sufficiently high to sustain acetylcholine synthesis in the pre-ganglionic nerve endings.

4.3. Catecholamine release induced by endogenous and exogenous acetylcholine

Either exogenous or endogenous acetylcholine evokes catecholamine release by activating cholinergic receptors on the surface of chromaffin cells (Douglas, 1975). The interstitial acetylcholine levels serves as an index of input into chromaffin cells. We examined whether the estimated interstitial acetylcholine levels were identical between exogenous acetylcholine and nerve stimulation when

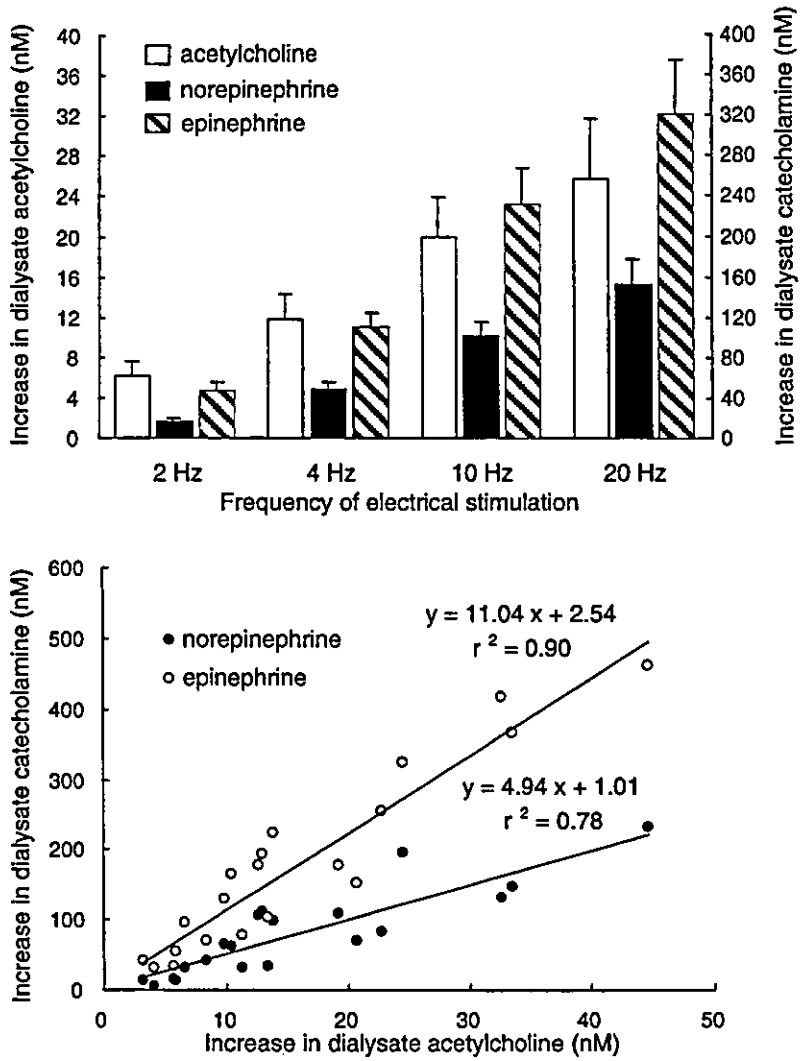

Fig. 2. (*Upper panel*) Dialysate acetylcholine response was enhanced from 6 ± 1 to 26 ± 6 nM when the frequency of nerve stimulation was increased from 2 to 20 Hz. Similarly, dialysate norepinephrine and epinephrine responses were enhanced from 16 ± 4 to 152 ± 26 nM and 48 ± 9 to 321 ± 54 nM, respectively, $n = 5$. Values are mean ± S.E. (*Lower panel*) The relationship between dialysate catecholamine response (*ordinate*) and dialysate acetylcholine response (*abscissa*) of five rats. Dialysate norepinephrine and epinephrine responses correlated with dialysate acetylcholine responses. These relations were expressed by regression equations with correlation coefficients of $y = 4.94x + 1.01$, $r^2 = 0.78$, and $y = 11.04x + 2.54$, $r^2 = 0.90$, respectively.

dialysate catecholamine responses were equal. Actually the estimated interstitial acetylcholine levels during nerve stimulation (2 Hz) were identical with those during acetylcholine infusion (10 μM). These data indicate that inputs into chromaffin cells were almost identical between the two stimulations. It could be inferred from this finding that dialysate acetylcholine concentration reflects acetylcholine levels at the surface of chromaffin cells and serves as an index of cholinergic transmission in the adrenal medulla.

4.4. Relationship of acetylcholine and catecholamine release

Dialysate norepinephrine and epinephrine responses were correlated with the frequency of splanchnic nerve stimulation. This norepinephrine and epinephrine release occurred as a consequence of acetylcholine release by splanchnic nerve stimulation. We found a linear relation between dialysate acetylcholine response and dialysate catecholamine responses. This indicates that the input–output relationship in the adrenal medulla is linear over the range of frequency from 2 to 20 Hz. Dialysate acetylcholine response of 1 nM evoked dialysate norepinephrine response of about 5 nM and dialysate epinephrine response of about 11 nM. This relation between dialysate acetylcholine and catecholamine responses could provide quantitative information about the input–output relationship in the adrenal medulla.

4.5. Effects of cholinergic receptor antagonists

It has been suggested that acetylcholine release from pre-ganglionic nerve endings is modulated by pre-synaptic

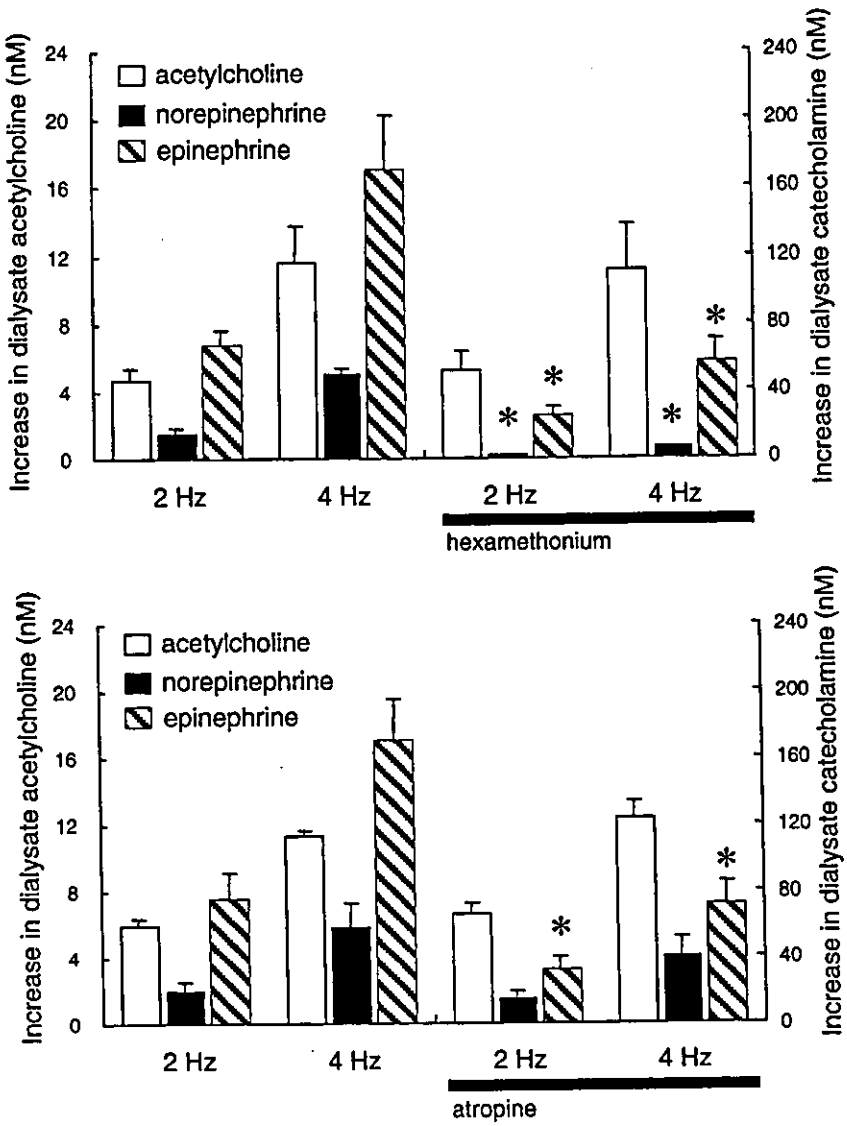

Fig. 3. (*Upper panel*) At both 2 and 4 Hz of nerve stimulation, hexamethonium suppressed dialysate norepinephrine and epinephrine responses, but did not affect acetylcholine response, $n = 5$. Values are mean ± S.E. $^*P < 0.05$ vs. concurrent dialysate norepinephrine or epinephrine response before administration of hexamethonium. (*Lower panel*) At both 2 and 4 Hz of nerve stimulation, atropine suppressed epinephrine response, but did not affect norepinephrine and acetylcholine responses, $n = 5$. Values are mean ± S.E. $^*P < 0.05$ vs. concurrent dialysate norepinephrine or epinephrine response before administration of atropine.

cholinergic autoreceptors (Dujic et al., 1990; Myers and Undem, 1996; Barbara et al., 1998). Neostigmine might induce the activation of pre-synaptic cholinergic receptors by increasing the acetylcholine levels in synaptic regions (Brehm et al., 1992) and suppress acetylcholine release by activating pre-synaptic autoreceptors. In the present study, neither hexamethonium nor atropine affected dialysate acetylcholine response to nerve stimulation at either 2 or 4 Hz. Thus, autoinhibition of acetylcholine release can be considered insignificant in our experimental condition, and dialysate acetylcholine response reflects pre-ganglionic nerve activities. In contrast, hexamethonium suppressed norepinephrine and epinephrine releases by nerve stimulation whereas atropine suppressed only epinephrine release. The muscarinic agonist, muscarine or pilocarpine preferentially enhanced epinephrine release (Douglas and Poisner, 1965; Wakade and Wakade, 1983). These results suggest that both nicotinic and muscarinic receptors exist on the surface of epinephrine-storing cells, while, on the surface of norepinephrine-storing cells, nicotinic receptors are primarily present.

4.6. Methodological limitations

We locally administered neostigmine to adrenal medulla through dialysis probe. Cholinesterase inhibitor was necessary to detect acetylcholine even during splanchnic nerve stimulation because released acetylcholine is rapidly

degraded by acetylcholinesterase before reaching the dialysis fiber. In the same preparation, local administration of neostigmine enhanced the dialysate catecholamine response to nerve stimulation by about three-fold, but did not influence the responses of heart rate and mean arterial pressure (Akiyama et al., 2003). Total catecholamine release from adrenal gland might not change by the local administration of neostigmine. In the present study, dialysate catecholamine response was correlated with the frequency of splanchnic nerve stimulation. Thus, in the presence of neostigmine, absolute value of dialysate catecholamine response is exaggerated, but could reflect relative changes in catecholamine release from adrenal gland.

Acknowledgements

This study was supported by the Program for Promotion of Fundamental Studies in Health Science of the Organization for Pharmaceutical Safety and Research (of Japan); by a Health Sciences Research Grant for Advanced Medical Technology from the Ministry of Health and Welfare of Japan; by a Ground-Based Research Grand for the Space Utilization promoted by NASDA (National Space Development Agency of Japan) and Japan Space Forum; by Grants-in-Aid for scientific research from the Ministry of Education, Science.

References

Akiyama, T., Yamazaki, T., 2000. Adrenergic inhibition of endogenous acetylcholine release on post-ganglionic cardiac vagal nerve terminals. Cardiovasc. Res. 46, 531–538.

Akiyama, T., Yamazaki, T., 2001. Effects of right and left vagal stimulation on left ventricular acetylcholine levels in the cat. Acta Physiol. Scand. 172, 11–16.

Akiyama, T., Yamazaki, T., Ninomiya, I., 1991. In vivo monitoring of myocardial interstitial norepinephrine by dialysis technique. Am. J. Physiol. 261, H1643–H1647.

Akiyama, T., Yamazaki, T., Ninomiya, I., 1994. In vivo detection of endogenous acetylcholine release in cat ventricles. Am. J. Physiol. 266, H854–H860.

Akiyama, T., Yamazaki, T., Mori, H., Sunagawa, K., 2003. Inhibition of cholinesterase elicits muscarinic receptor-mediated synaptic transmission in the rat adrenal medulla. Auton. Neurosci.: Basic Clin. 107, 65–73.

Barbara, J.G., Lemos, V.S., Takeda, K., 1998. Pre- and post-synaptic muscarinic receptors in thin slices of rat adrenal gland. Eur. J. Neurosci. 10, 3535–3545.

Brehm, G., Lindmar, R., Löffelholz, K., 1992. Inhibitory and excitatory muscarinic receptors modulating the release of acetylcholine from the post-ganglionic parasympathetic neuron of the chicken heart. Naunyn-Schmiedeberg's Arch. Pharmacol. 346, 375–382.

Calabresi, P., Centonze, D., Gubellini, P., Pisani, A., Bernardi, G., 2000. Acetylcholine-mediated modulation of striatal function. Trends Neurosci. 23, 120–126.

Collier, B., 1977. Biochemistry and physiology of cholinergic transmission. In: Handbook of Physiology. The Nervous System. Cellular Biology of Neurons, Section 1, Part 1. Amercian Physiological Soceity, Bethesda, MD, Chapter 13, pp. 463–492.

Collier, B., Johnson, G., Kirpekar, S.M., Prat, J., 1984. The release of acetylcholine and of catecholamine from the cat's adrenal gland. Neuroscience 13, 957–964.

Coupland, R.E., 1965. The Natural History of the Chromaffin Cell. Longmans, London.

Coupland, R.E., Parker, T.L., Kesse, W.K., Mohamed, A.A., 1989. The innervation of the adrenal gland. Part III. Vagal innervation. J. Anat. 163, 173–181.

Douglas, W.W., 1975. Secretomotor control of adrenal medullary secretion: synaptic, membrane, and ionic events in stimulus–secretion coupling. In: Handbook of Physiology. Endocrinology. Adrenal Gland, Section 7, vol. VI. Amercian Physiological Soceity, Bethesda, MD, Chapter 26, pp. 367–388.

Douglas, W.W., Poisner, A.M., 1965. Preferential release of adrenaline from the adrenal medulla by muscarine and pilocarpine. Nature 208, 1102–1103.

Dujic, Z., Roerig, D.L., Schedewie, H.K., Kampine, J.P., Bosnjak, Z.J., 1990. Presynaptic modulation of ganglionic ACh release by muscarinic and nicotinic receptors. Am. J. Physiol. 259, R288–R293.

Fibiger, H.C., 1991. Cholinergic mechanisms in learning, memory and dementia: a review of recent evidence. Trends Neurosci. 14, 220–223.

Holman, M.E., Coleman, H.A., Tonta, M.A., Parkington, H.C., 1994. Synaptic transmission from splanchnic nerves to the adrenal medulla of guinea-pigs. J. Physiol. 478, 115–124.

Kawada, T., Yamazaki, T., Akiyama, T., Shishido, T., Inagaki, M., Uemura, K., Miyamoto, T., Sugimachi, M., Takaki, H., Sunagawa, K., 2001. In vivo assessment of acetylcholine-releasing function at cardiac vagal nerve terminals. Am. J. Physiol. 281, H139–H145.

Lewis, P.R., Shute, C.C., 1969. An electron-microscopic study of cholinesterase distribution in the rat adrenal medulla. J. Microsc. 89, 181–193.

Myers, A.C., Undem, B.J., 1996. Muscarinic receptor regulation of synaptic transmission in airway parasympathetic ganglia. Am. J. Physiol. 270, L630–L636.

Niijima, A., 1992. Electrophysiological study on the vagal innervation of the adrenal gland in the rat. J. Auton. Nerv. Syst. 41, 87–92.

O'Farrell, M., Ziogas, J., Marley, P.D., 1997. Effects of N- and L-type calcium channel antagonists and (±)-Bay K8644 on nerve-induced catecholamine secretion from bovine perfused adrenal glands. Br. J. Pharmacol. 121, 381–388.

Palkama, A., 1967. Demonstration of adrenomedullary catecholamines and cholinesterases at electron microscopic level in the same tissue section. Ann. Med. Exp. Biol. Fenn. 45, 295–306.

Parker, T.L., Kesse, W.K., Mohamed, A.A., Afework, M., 1993. The innervation of the mammalian adrenal gland. J. Anatom. 183, 265–276.

Somogyi, P., Chubb, I.W., Smith, A.D., 1975. A possible structural basis for the extracellular release of acetylcholinesterase. In: Proceedings of the Royal Society of London, Series B. Biol. Sci. 191, 271–283.

Taylor, P., Brown, J.H., 1998. Acetylcholine. In: Siegel, G., Agranoff, B., Albers, R., Fisher, S., Uhler, M. (Eds.), Basic Neurochemistry, sixth ed. Lippincott–Raven, Philadelphia–New York, pp. 213–242.

Wakade, A.R., Wakade, T.D., 1983. Contribution of nicotinic and muscarinic receptors in the secretion of catecholamines evoked by endogenous and exogenous acetylcholine. Neuroscience 10, 973–978.

Winer, B.J., 1971. Statistical Principles in Experimental Design, Second ed. McGraw-Hill, New York.

Role of Calcineurin B Homologous Protein in pH Regulation by the Na^+/H^+ Exchanger 1: Tightly Bound Ca^{2+} Ions as Important Structural Elements†

Tianxiang Pang,‡ Takashi Hisamitsu,‡ Hidezo Mori,⊥ Munekazu Shigekawa,§ and Shigeo Wakabayashi*,‡

‡*Department of Molecular Physiology and Department of Cardiac Physiology, National Cardiovascular Center Research Institute, Suita, Osaka 565-8565, Japan, and Department of Human Life Sciences, Senri Kinran University, Suita, Osaka 565-0873, Japan*

Received November 10, 2003; Revised Manuscript Received January 27, 2004

ABSTRACT: We studied the role of the interaction of calcineurin homologous protein 1 (CHP1) with the Na^+/H^+ exchanger 1 (NHE1), particularly its EF-hand Ca^{2+} binding motifs, in the intracellular pH (pH_i)-dependent regulation of NHE1. We found that $^{45}Ca^{2+}$ binds to two EF-hand motifs (EF3 and 4) of the recombinant CHP1 proteins with high affinity (apparent K_d = ~90 nM). Complex formation between CHP1 and the CHP1 binding domain of NHE1 resulted in a marked increase in the Ca^{2+} binding affinity (K_d = ~2 nM) by promoting a conformational change of the EF-hands toward the tightly Ca^{2+}-bound form. This suggests that CHP1 always contains two Ca^{2+} ions when associated with NHE1 in cells. Interestingly, overexpression of GFP-tagged CHP1 with mutations in EF3 or EF4 significantly reduced the exchange activity in the neutral pH_i range and partly impaired the activation of NHE1 in response to various stimuli, such as growth factors and osmotic stress. Furthermore, we found that, in addition to reducing the activity (V_{max}), a CHP1 binding-defective NHE1 mutant had a marked reduction in pH_i sensitivity (~0.7 pH unit acidic shift), which consequently abolished various regulatory responses of NHE1. These observations suggest that the association of NHE1 with CHP1 is crucial for maintenance of the pH_i sensitivity of NHE1 and that tightly bound Ca^{2+} ions may serve as important structural elements in the "pH_i sensor" of NHE1.

The Na^+/H^+ exchanger (NHE1[1]) proteins in the plasma membrane and various organellar compartments of mammalian cells catalyze the electroneutral countertransport of Na^+ for H^+. Nine distinct isoforms of the Na^+/H^+ exchanger (NHE1 to NHE9) have been isolated to date, and these molecules have been shown to exhibit similar membrane topologies with 12 predicted N-terminal membrane-spanning helices and a large C-terminal cytoplasmic region (*1*−*10*). They show considerable differences in their tissue expression patterns, membrane localization, and kinetic and pharmacological properties. The plasma membrane exchangers (NHE1−5) are primarily involved in regulation of intracellular pH and Na^+ concentration, but they also participate in a broad range of physiological processes, such as cell volume regulation, transepithelial transport of electrolytes, cell proliferation, apoptosis, and differentiation (*1*−*3*).

Of the nine isoforms identified to date, NHE1 has been characterized in the most detail. NHE1 is ubiquitously expressed in essentially all tissues and cell types and plays a major role in maintaining intracellular pH and cell volume homoeostasis. The activity of NHE1 is controlled by various extrinsic factors, including growth factors, hormones, and mechanical stimuli (*1*−*3*). A variety of signaling molecules regulate the NHE1 protein, such as calcinuerin B homologous protein (CHP) (*11*−*13*), Ca^{2+}/calmodulin (*14*, *15*), the low molecular weight GTPases Ras and Rho (*16*), p42/44 mitogen-activated protein kinases (*17*), p90 ribosomal S6 kinase (*18*), 14-3-3 protein (*19*), Nck-interacting kinase (*20*), phosphatidylinositol 4,5-bisphosphate (*21*), and carbonic anhydrase II (22). Recently, we have focused on the role of CHP in regulation of the activities of the Na^+/H^+ exchangers (*12*, *13*).

CHP was initially discovered as a protein (p22) involved in vesicular transport (*23*), as well as a molecule that interacted with NHE (*11*). Since then, CHP has been reported

† This work was supported by Grant-in-Aid for Priority Areas 13142210 and Grant-in-Aid 14580664 for Scientific Research from the Ministry of Education, Science, and Culture of Japan, by the promotion of Fundamental Studies in Health Science of the Organization for Pharmaceutical Safety and Research of Japan (Promotion of Fundamental Studies in Health Science), and by Grant nano-001 for Research on Advanced Medical Technology from the Ministry of Health, Labor, and Welfare of Japan. T.P. was supported by a Japan Society for the Promotion of Science Postdoctoral Fellowship.

* To whom correspondence should be addressed. Department of Molecular Physiology, National Cardiovascular Center Research Institute, Fujishirodai 5-7-1, Suita, Osaka 565-8565 Japan. Tel: +81-6-6833-5012. Fax: +81-6-6835-5314. E-mail: wak@ri.ncvc.go.jp.

‡ Department of Molecular Physiology, National Cardiovascular Center Research Institute.

⊥ Department of Cardiac Physiology, National Cardiovascular Center Research Institute.

§ Senri Kinran University.

[1] Abbreviations: NHE, Na^+/H^+ exchanger; CHP, calcineurin B homologous protein; GFP, green fluorescent protein; CaN, calcineurin; CaM, calmodulin; pH_i, intracellular pH; EIPA, 5-(*N*-ethyl-*N*-isopropyl)-amiloride; DMEM, Dulbecco's modified Eagle's medium; HEPES, 2-[4-(2-hydroxyethyl)-1-piperazinyl]ethansulfonic acid; Tris, Tris(hydroxymethyl)aminomethane; EGTA, *O*,*O*′-bis(2-aminoethyl)ethylene glycol-*N*,*N*,*N*′,*N*′-tetraacetic acid; PBS, phosphate-buffered saline; PDGF-BB, platelet-derived growth factor-BB; PMA, phorbol 12-myristate 13-acetate; SDS−PAGE, sodium dodecyl sulfate−polyacrilamide gel electrophoresis.

10.1021/bi0360004 CCC: $27.50
Published on Web 03/06/2004

to exhibit multiple functions, including inhibition of calcinuerin phosphatase activity (*24*), as well as interaction with microtubules (*25*), DRAK2 (death-associated protein kinase related apoptosis inducing protein kinase 2) (*26*) and KIF1Bβ2 (kinesin-family 1Bβ2) (*27*). Previously, we reported that the ubiquitous CHP isoform (designated as CHP1) is an essential cofactor for the physiological activity of the Na^+/H^+ exchanger by interacting with the juxtamembrane region in the C-terminal cytoplasmic domain of plasma membrane exchanger isoforms (*12*). Furthermore, we reported that the second CHP isoform (CHP2) might be involved in maintenance of the abnormally high pH_i in malignantly transformed cells (*13*). CHP2 is expressed at a relatively high level in the rat small intestine (*28*), suggesting that it plays a specific role in this tissue. These CHP proteins contain four EF-hand Ca^{2+} binding motifs and are myristoylated at the N-terminus (Gly^2). In addition, CHP1 is phosphorylated in cells in a serum-dependent manner (*11*). However, the roles of these posttranslational modifications of CHP proteins in the pH_i-dependent regulation or acute activation of NHE in response to extracellular stimuli are largely unknown, although this protein family appears to be essential for the physiological exchange activity of plasma membrane NHEs.

In this study, we focused on the EF-hand Ca^{2+} binding motifs of CHP1. We found that the affinity of CHP1 for Ca^{2+} markedly (approximately 40-fold) increases upon complex formation with NHE1, probably by promoting a change in the conformation of the EF-hand motifs. The extremely low Ca^{2+} dissociation constant (~2 nM) of CHP1 suggests that Ca^{2+} ions remain tightly bound to CHP1 when it is complexed with NHE1 in the plasma membrane. On the basis of properties of various CHP1 and NHE1 mutant proteins in cells, we suggest that CHP1 is important for pH_i-dependent regulation of NHE1 and that tightly bound Ca^{2+} ions play an important role in maintaining a structure that is critical for this function of CHP1.

EXPERIMENTAL PROCEDURES

Materials. The amiloride derivative EIPA was a gift from the New Drug Research Laboratories of Kanebo, Ltd. (Osaka, Japan). $^{45}CaCl_2$, $^{22}NaCl$, and ^{14}C-benzoic acid were purchased from Dupont-NEN (Boston, MA). The rabbit polyclonal antibodies against CHP1 and NHE1 were described previously (*12*, *14*). All other chemicals were of the highest purity available.

Cells, Culture Conditions, and Stable Expression. The exchanger-deficient cell line PS120 (*29*) and corresponding transfectants were maintained in DMEM (Life Technologies Inc., Rockville, MD) containing 25 mM $NaHCO_3$ and supplemented with 7.5% (v/v) fetal calf serum, penicillin (50 units/mL), and streptomycin (50 μg/mL). Cells were maintained at 37 °C in the presence of 5% CO_2. PS120 cells (5×10^5 cells/100-mm dish) were transfected with each plasmid construct (20 μg) by the calcium phosphate coprecipitation technique. Cell populations stably expressing wild-type or mutant human NHE1 were selected by the H^+-killing procedure as described previously (*30*). Cells stably overexpressing GFP-tagged CHP1 were first selected with G418, and then single colonies were selected by monitoring GFP fluorescence.

Construction of Expression Vectors. All the constructs were produced by means of a polymerase chain reaction (PCR)-based strategy. For construction of GFP-tagged CHP1 or its mutant forms with mutations in Ca^{2+} binding motifs or in the myristoylated glycine (G2A), a cDNA encoding CHP1 was cloned into the mammalian expression vector pEGFP-N1 (Clontech, Palo Alto, CA). The plasmids carrying cDNAs for the wild-type or mutant NHE1s were all cloned into the mammalian expression vector pECE. Constructs were confirmed by sequencing plasmids with an ABI-PRISM DNA sequencer model 3100 (Applied Biosystems, Foster City, CA).

Purification of Recombinant Proteins. Recombinant histidine-tagged CHP1 proteins were produced in *Escherichia coli* (BL21-Star; Invitrogen, San Diego, CA) transformed with pET11 carrying the cDNA encoding CHP1 containing the C-terminal six histidine residues as described previously (*12*). Myristoylated CHP1 was produced using the same bacteria except they also contained the vector pBB131, which carries the yeast *N*-myristoyltransferase cDNA (kindly provided by Dr. J. I. Gordon, Washington University). Myristoylation of CHP1 (or p22) produced by this method was previously confirmed (*23*). For production of the complex of CHP1 and the CHP1 binding region of NHE1, the cytoplasmic region (aa 503−545) of NHE1 was cloned into the vector pET24 and coexpressed with His-tagged CHP1 in *E. coli* in the presence of ampicillin and kanamycin. Myristoylated and nonmyristoylated CHP1 proteins and CHP1/NHE1 (aa 503−545) complex proteins were all recovered in the soluble fraction and partially purified by passage through a Ni^{2+} affinity resin column (ProBond, Invitrogen) according to the manufacturer's protocol. Partially purified CHP1 proteins were found to be ~70% pure. We did not carry out further purification of CHP1 because of aggregation during storage. The complexes consisting of CHP1 or its mutant variants complexed with the NHE1 fragment were further purified to more than 95% by diethylaminoethyl-Sepharose column chromatography. All the proteins were dialyzed overnight against 60 mM KCl and 10 mM HEPES/Tris (pH 7.2).

Measurement of Equilibrium $^{45}Ca^{2+}$ Binding. $^{45}Ca^{2+}$ binding to the proteins was measured by a filtration method as described previously (*31*). Purified proteins (0.1−0.2 mg/mL) were incubated for 1 h at 25 °C in a solution containing 60 mM KCl, 5 mM $MgCl_2$, 50 μM $CaCl_2$, 0.02 μCi/mL $^{45}CaCl_2$, 10 mM HEPES/Tris (pH 7.2), and different concentrations of EGTA (0−58 mM), giving a free Ca^{2+} concentration of 0.1 nM to 50 μM. Aliquots (1 mL) of the reaction mixture were transferred onto 0.22-μm Millipore filters (Millipore, Bedford, MA) and filtered under vacuum. As controls, the same reaction mixtures without proteins were filtered to measure the background binding of ^{45}Ca by the filters. More than 95% of the proteins were retained in the filters. After the filters were dried, ^{45}Ca radioactivity was measured by scintillation counting.

Measurement of $^{45}Ca^{2+}$ Release from Proteins. $^{45}Ca^{2+}$ release from proteins was measured using a rapid filtration apparatus as described previously (*31*). After preincubation of proteins with a solution containing 50 μM $^{45}CaCl_2$ for 1 h, aliquots (1 mL) of reaction mixtures were filtered through Millipore filters. Filters were washed at a constant rate (0.2−2 mL/s) for the indicated periods (0.2−30 s) with

0.4−6 mL of 60 mM KCl, 5 mM $MgCl_2$, 10 mM HEPES/Tris (pH 7.2), and 10 mM EGTA. After the filters were dried, ^{45}Ca radioactivity was measured by scintilation counting.

Immunoprecipitation and Immunoblotting. Immunoprecipitation and immunoblotting were performed essentially as described previously (*14*). Briefly, cells were solubilized with 1% Triton X-100 in a solution of 150 mM NaCl, 10 mM HEPES-Tris (pH 7.4), and protease inhibitors. Cell lysates were incubated with respective antibodies and protein A Sepharose. After centrifugation, precipitated materials were separated on 7.5% or 12% polyacrylamide gels and electrophoretically transferred to Immobilon membranes (Millipore). After blocking, incubation with antibodies and washing, protein signals were visualized by enhanced chemiluminescence (Amersham, Buckinghamshire, U.K.). The signal intensity was measured using a photonic microscope system (ARUGUS-100, Hamamatsu photonics).

Measurement of $^{22}Na^+$ Uptake. $^{22}Na^+$ uptake activity and its pH_i dependence were measured by the K^+/nigericin pH_i clamp method essentially as described previously (*32*). Serum-depleted cells in 24-well dishes were incubated for 30 min at 37 °C in Na^+-free choline chloride/KCl medium containing 20 mM HEPES/Tris (pH 7.4), 1.2−140 mM KCl, 2 mM $CaCl_2$, 1 mM $MgCl_2$, 5 mM glucose (or 5 mM 2-deoxyglucose plus 2 μg/mL oligomycin under conditions of ATP depletion), and 5 μM nigericin. $^{22}Na^+$ uptake was started by adding the same choline chloride/KCl solution containing $^{22}NaCl$ (37 kBq/mL, final concentration = 1 mM), 1 mM ouabain, and 100 μM bumetanide. In some wells, 0.1 mM EIPA was added to the solution. After 1 min, cells were washed four times with ice-cold PBS to terminate $^{22}Na^+$ uptake. The pH_i was calculated from the imposed K^+ concentration gradient by assuming the equilibrium $[K^+]_i/[K^+]_o = [H^+]_o/[H^+]_i$ and an intracellular K^+ concentration of 120 mM. Data were normalized according to the protein concentration as measured by the bicinchoninic assay (Pierce Chemical Co., IL) using bovine serum albumin as a standard.

Measurement of pH_i. Changes in pH_i were measured by the [^{14}C]-benzoic acid equilibration method (*30*). For this measurement, serum-depleted cells were incubated for 30 min in bicarbonate-free HEPES-buffered DMEM (pH 7.0) and then incubated in the same medium containing [^{14}C]-benzoic acid (37 kBq/mL) for 20 min at 37 °C. After the cells were washed four times with ice-cold PBS, ^{14}C-radioactivity taken up by cells was measured. Changes in pH_i were calculated as described previously (*30*).

Statistics. Data of the pH dependence of EIPA-sensitive $^{22}Na^+$ uptake were simulated by fitting the values to the sigmoidal dose-response equation, rate of EIPA-sensitive $^{22}Na^+$ uptake = $V_{max}/(1 + 10^{\log(pK - pH_i)n})$ (pK = pH_i giving half-maximal $^{22}Na^+$ uptake; n = Hill coefficient), using the simulation program included in Graphpad Prizm (Microsoft Corp., Redmond, WA). Equilibrium $^{45}Ca^{2+}$ binding was fitted to the dose−response equation, $^{45}Ca^{2+}$ bound = maximal $^{45}Ca^{2+}$ bound/$(1 + (K_d - [Ca^{2+}])^n)$ (K_d = apparent dissociation constant for Ca^{2+}; n = Hill coefficient). Kinetic parameters were expressed as the best fit values with standard errors, whereas other data were expressed as the means ± SD for at least three determinations.

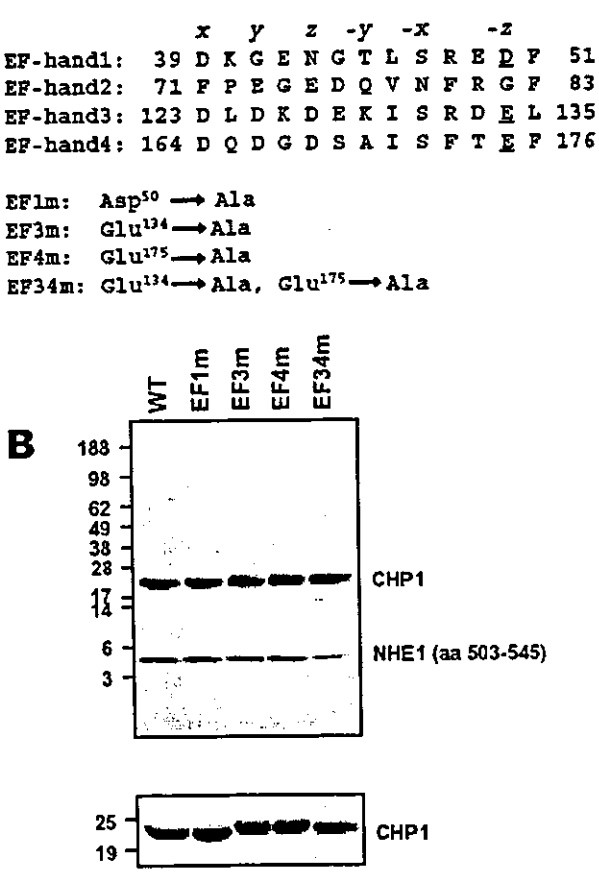

FIGURE 1: Amino acid sequences of EF-hand motifs and purified proteins of various CHP1 mutants. Panel A shows amino acid sequences of four EF-hand motifs present in CHP1. In four mutant CHP1s (EF1m, EF3m, EF4m, and EF34m), Asp^{50}, Glu^{134}, Glu^{175}, and both Glu^{134}/Glu^{175} were replaced by alanine. In panel B, the purified complex of His-tagged CHP1 with the NHE1 segment (aa 503−545) (10 μg) was separated by electrophoresis on a 4−15% gradient (upper panel) or 12% SDS−PAGE gel (lower panel) and then visualized by Coomassie Brilliant Blue staining.

RESULTS

Characterization of Ca^{2+} Binding Motifs in CHP1. We first analyzed $^{45}Ca^{2+}$ binding to EF-hand motifs of CHP1 using recombinant CHP1 and its complex with the binding domain in NHE1. CHP1 interacts with NHE1 at the juxtamembrane region of the carboxyl-terminal cytoplasmic domain of NHE1. Hydrophobic residues of NHE1, such as Phe^{526}, Leu^{527}, Leu^{530}, and Leu^{531}, were shown to be important for the interaction of CHP1 with NHE1 (*12*). CHP1 contains four potential EF-hand Ca^{2+} binding motifs, of which two ancestral sites (EF1 and -2) may not bind Ca^{2+} due to substitution of critical acidic residues (Figure 1A). The canonical EF-hand consists of 29 consecutive residues with two flanking helices and a 12-residue loop (Figure 1A). The chelating loop residues in positions 1 (+x), 3 (+y), 5 (+z), 7 (−y), 9 (−x), and 12 (−z) ligate Ca^{2+} through seven oxygen atoms arranged three-dimensionally on the axes of a pentagonal bipyramid (*33*, *34*). The −z position, providing the only side chain oxygen atoms, is crucial for Ca^{2+} binding (*33*−*35*). To characterize these Ca^{2+} binding motifs, we introduced mutations into EF1, -3, and -4 in which acidic residues (aspartic acid or glutamic acid) at the −z position were replaced by alanine (Figure 1B). We coexpressed the wild-type or mutant CHP1s together with the juxtamembrane region of NHE1 (aa 503−545) in *E. coli*. We confirmed that

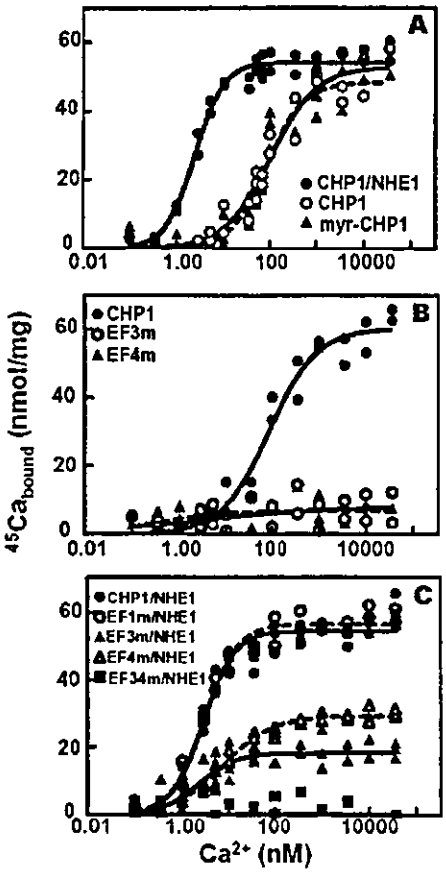

FIGURE 2: Equilibrium $^{45}Ca^{2+}$ binding to various CHP1 mutant proteins. In panels A–C, CHP1 or its various mutant proteins and the complex of CHP1 variants with the NHE1 segment (aa 503–545) (0.1–0.2 mg/mL) were incubated for 1 h in solutions containing 50 μM $^{45}CaCl_2$ and various concentrations of EGTA, which produce 0.2 nM to 50 μM free Ca^{2+}. Symbols corresponding to each protein variant were indicated in figures. The solutions were filtered through Millipore filters, and $^{45}Ca^{2+}$ bound to the CHP1 proteins was measured.

the purified complex proteins (>95% pure) of the wild-type CHP1, EF1m, EF3m, or EF4m with aa 503–545 of NHE1 were retained as a single peak on gel filtration chromatography and contained the CHP1 variant and the NHE1 peptide at a 1:1 molar ratio (data not shown). In addition, using 4–15% polyacrylamide gradient gels, we confirmed that the purified samples mostly contained comparable molar amounts of the CHP1 variant and the NHE1 fragment (Figure 1B, upper panel). However, in EF34m with double mutations at EF3 and -4, the amount of the NHE1 fragment was significantly reduced, suggesting that this double mutation impairs the interaction of CHP1 with NHE1. On 12% SDS–PAGE, EF3m, EF4m, and EF34m proteins were found to migrate more slowly than the wild-type or EF1m proteins (Figure 1B, lower panel), suggesting that a mutation-induced conformational change occurred in these three mutant proteins that had impaired Ca^{2+} binding (see below).

We measured $^{45}Ca^{2+}$ binding to various CHP1 mutant proteins by a membrane filtration procedure. We found that $^{45}Ca^{2+}$ bound to the partially purified CHP1 proteins with an apparent K_d of ~90 nM (Figure 2A and Table 1). The maximal amount of $^{45}Ca^{2+}$ bound to CHP1 corresponded to ~2 mol of Ca^{2+} bound/mol of CHP1, assuming that the CHP1 sample was 70% pure. Myristoylation did not significantly affect the apparent affinity for Ca^{2+} nor the

Table 1: Parameters for Equilibrium $^{45}Ca^{2+}$ Binding

proteins	apparent K_d ± SE (nM)[a]	Hill coefficient ± SE
CHP1	89.9 ± 9.3	0.77 ± 0.12
myr-CHP1	86.4 ± 8.9	0.94 ± 0.17
CHP1/NHE1	2.32 ± 0.18	1.22 ± 0.15
EF1m/NHE1	2.17 ± 0.39	0.98 ± 0.14
EF3m/NHE1	2.89 ± 0.28	1.27 ± 0.55
EF4m/NHE1	2.24 ± 0.26	0.76 ± 0.09

[a] The data shown in Figure 2 were fitted to the equation for equilibrium $^{45}Ca^{2+}$ binding as described in Experimental Procedures.

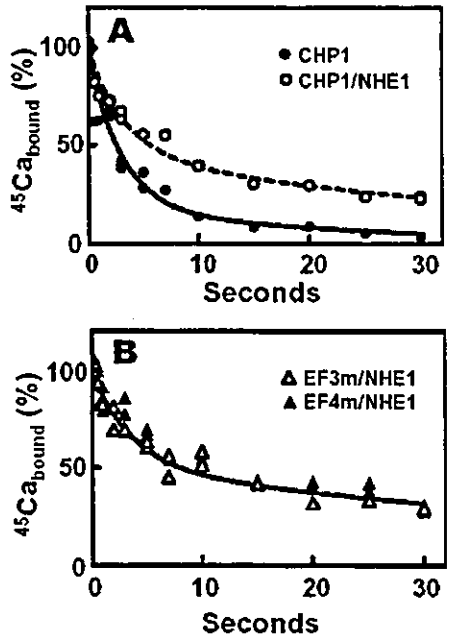

FIGURE 3: Time courses of $^{45}Ca^{2+}$ release from CHP1 proteins: (A) $^{45}Ca^{2+}$ release from CHP1 alone (●) or CHP1/NHE1 complex (○); (B) $^{45}Ca^{2+}$ release from EF3m/NHE1 (△) or EF4m/NHE1 complex (▲). CHP1 proteins or the complex of CHP1 variants with the NHE1 segment (aa 503–545) (0.1–0.2 mg/mL) were incubated for 1 h in a solution containing 50 μM $^{45}CaCl_2$, applied to Millipore filters, and washed with a solution containing EGTA. $^{45}Ca^{2+}$ remaining on the filters was measured.

maximal level of $^{45}Ca^{2+}$ binding (Figure 2A and Table 1). Interestingly, when CHP1 formed a complex with the NHE1 fragment, the binding affinity for $^{45}Ca^{2+}$ increased markedly (~40-fold, Figure 2A and Table 1). The extremely low apparent dissociation constant (~2 nM) deviates substantially from the physiological cytosolic Ca^{2+} concentration of cells (0.1–10 μM). The maximal level of Ca^{2+} binding on the complex again corresponded to ~2 mol of Ca^{2+} bound/mol of CHP1. Mutation of either of Ca^{2+} binding motifs EF3 or EF4, but not EF1, resulted in loss of approximately 1 mol of $^{45}Ca^{2+}$ bound to the complex (Figure 2C). On the other hand, $^{45}Ca^{2+}$ binding was completely blocked when the experiment was carried out using EF3m and EF4m proteins but without the NHE1 fragment (Figure 2B) or when two sites were simultaneously mutated (EF34m) (Figure 2C). Together, these results indicate that CHP1 binds two Ca^{2+} ions, one at EF3 and the other at EF4.

To determine how complex formation increases the Ca^{2+} binding affinity, we measured $^{45}Ca^{2+}$ release from CHP1 proteins by rapid filtration. As shown in Figure 3A, most of the $^{45}Ca^{2+}$ bound to CHP1 without the NHE1 fragment was released rapidly ($t_{1/2}$ = ~2 s). In contrast, $^{45}Ca^{2+}$ release from

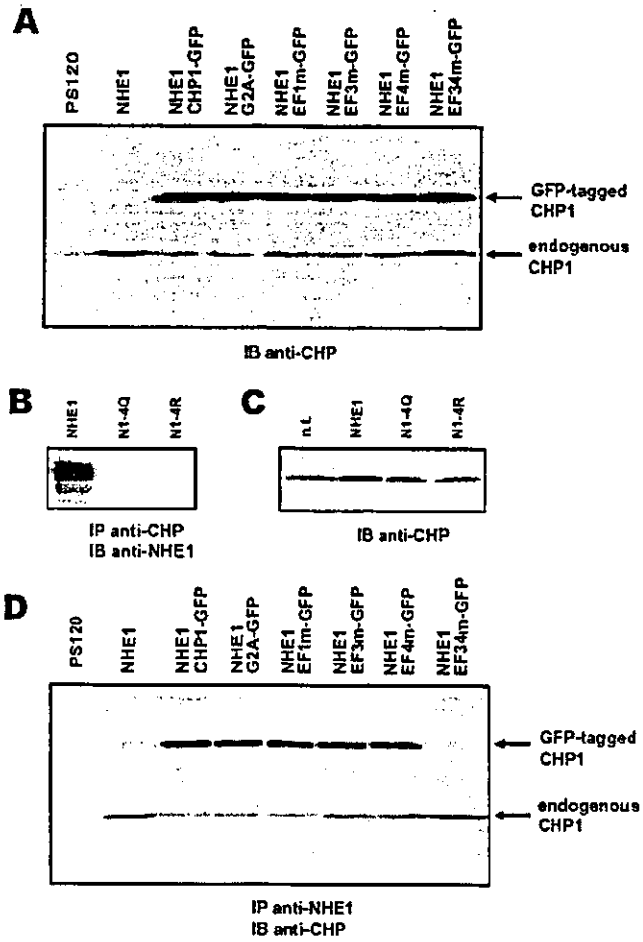

FIGURE 4: Expression of various GFP-tagged CHP1 proteins and their coimmunoprecipitation with NHE1. Panel A shows the expression level of GFP-tagged CHP1 and its variants (indicated at the top of the figure). Cell lysates (50 μg) from stable transfectants were subjected to SDS−PAGE, and expression of endogenous and exogenous CHP1 proteins were detected by immunoblotting (IB) with an anti-CHP1 antibody. A result for untransfected PS120 cells is shown in the first lane. Panel B shows coimmunoprecipitation of the wild-type or mutant (4Q and 4R) exchangers with endogenous CHP1. Lysates from cells stably expressing these exchangers were subjected to immunoprecipitation with anti-CHP1 antibody followed by immunoblotting with anti-NHE1 antibody. Panel C shows the expression level of endogenous CHP1 in cells expressing the wild-type or mutant NHE1s: n.t., no transfection. Panel D shows coimmunoprecipitation of CHP1 proteins with NHE1. Lysates from cells stably expressing various proteins were subjected to immunoprecipitation with anti-NHE1 antibody followed by immunoblotting with anti-CHP1 antibody. Note that in lanes from cells not transfected with GFP-tagged CHP1 (left two lanes), IgG protein bands were visible at the same positions as GFP-tagged CHP1.

CHP1 complexed with the NHE1 fragment ($t_{1/2}$ = ~7 s) was much slower. A slow release of $^{45}Ca^{2+}$ also occurred in two mutant CHP1 proteins, EF3m and EF4m, complexed with the NHE1 fragment (Figure 3B), suggesting that Ca^{2+} binds tightly to each EF hand.

Effects of CHP1 Mutations on NHE1 Regulation. To study the role of Ca^{2+} binding in NHE1 regulation by CHP1, we transfected GFP-tagged CHP1 into cells expressing NHE1 and obtained cells stably coexpressing these proteins. The results indicated that GFP-tagged CHP1 and its mutant derivatives were highly coexpressed in NHE1 transfectants (Figure 4A). Interestingly, expression of NHE1 markedly increased the level of expression of the endogenous CHP1 (3.6-fold), while coexpression of various GFP-tagged CHP1 variants, with the exception of CHP1-EF34m-GFP, reduced it (Table 2).

Table 2: Relative Amounts of Expressed GFP-Tagged CHP1 and Endogenous CHP1

transfected proteins	relative amount of GFP-tagged CHP1[a]	relative amount of endogenous CHP[b]
untransfected		1.00 ± 0.08
NHE1		3.63 ± 0.81[c]
NHE1 + CHP1-GFP	1.00 ± 0.11	1.11 ± 0.13
NHE1 + G2A-GFP	1.08 ± 0.11	1.03 ± 0.16
NHE1 + EF1m-GFP	0.93 ± 0.06	1.07 ± 0.11
NHE1 + EF3m-GFP	0.97 ± 0.11	1.15 ± 0.16
NHE1 + EF4m-GFP	1.06 ± 0.07	1.09 ± 0.10
NHE1 + EF34m-GFP	0.94 ± 0.12	3.85 ± 0.45[c]
NHE1-4Q		1.02 ± 0.09
NHE1-4R		1.03 ± 0.06

[a] The density of visualized protein bands on immunoblots (cf. Figure 4, panels A and C) is represented as values normalized according to the band density from cells expressing CHP1-GFP. Data are means ± SD (n = 3). [b] The band density is represented as values normalized according that from untransfected PS120 cells. Data are means ± SD (n = 3). [c] $P < 0.05$ versus control.

We further examined the effect of expression of CHP1 binding-defective NHE1 mutants 4Q and 4R on the amount of endogenous CHP. These mutant exchangers do not bind CHP1 as shown by coimmunoprecipitation studies (Figure 4B). The level of expression of the endogenous CHP1 did not increase on coexpression of these mutant exchangers (Figure 4B,C, Table 2). Thus, the amount of endogenous CHP1 in cells is highly dependent on expression of NHE1 and GFP-tagged CHP1.

Figure 4D shows the results for coimmunoprecipitation experiments using NHE1- and CHP1-specific antibodies to determine interactions of the expressed CHP1−GFP with NHE1. Anti-NHE1 antibody immunoprecipitated endogenous CHP1 from cells expressing NHE1. In cells coexpressing GFP−CHP1 and NHE1, the same antibody coimmunoprecipitated large quantities of GFP−CHP1 or its derivatives, and at the same time, the amount of immunoprecipitated endogenous CHP1 was markedly reduced. In cells coexpressing EF34m−GFP and NHE1, anti-NHE1 antibody coimmunoprecipitated the endogenous CHP1 but not exogenous GFP-tagged mutant CHP1, consistent with the findings of in vitro binding studies indicating that double mutation at EF3 and EF4 impairs the interaction of CHP1 with NHE1.

We next examined the subcellular localization of GFP-tagged CHP1. As reported previously (*12*), the GFP-tagged CHP1 is localized in the plasma membrane in cells coexpressing NHE1 (Figure 5A). Consistent with the in vitro binding data (Figure 1B), the GFP fluorescence was observed in the plasma membrane in cells coexpressing GFP-tagged CHP1 mutants except EF34m with NHE1 (Figure 5A; data not shown for G2A and EF1m). These results, together with the data from coimmunoprecipitation experiments, indicate that the endogenous CHP1 bound to NHE1 was efficiently replaced by expressed GFP-tagged wild-type or CHP1 mutants. However, the double mutant EF34m was not localized at the plasma membrane (Figure 5A) because of the weak interaction of this mutant protein with the juxtamembrane region of NHE1. We observed that GFP fluorescence was still observed in the plasma membrane after addition of phorbol ester, serum, thrombin, lysophosphatidic